The Pennsylvania State University

The Graduate School

EXPERIMENTAL STUDY OF GAS-LIQUID DIFFUSION IN POROUS ROCKS AND BULK FLUIDS

A Thesis in

Energy and Mineral Engineering

by

Xuanqing Lou

Submitted in Partial Fulfillment
of the Requirements
for the Degree of

Master of Science

August 2019

The thesis of Xuanqing Lou was reviewed and approved* by the following:

Zuleima T. Karpyn

Professor of Petroleum and Natural Gas Engineering
Quentin E. and Louise L. Wood Faculty Fellow in Petroleum and Natural Gas Engineering
Thesis Advisor

Luis F. Ayala H.

William A. Fustos Family Professor of Petroleum and Natural Gas Engineering
Associate Department Head for Graduate Education

Hamid Emami-Meybodi

Assistant Professor of Petroleum and Natural Gas Engineering

*Signatures are on file in the Graduate School

ABSTRACT

The design of oil recovery processes by gas injection or vapor solvent relies on knowledge of diffusion coefficients to enable meaningful production predictions. However, lab measurements of diffusion coefficients are often performed on bulk fluids, without accountability for the hindrance caused by the pore network structure and tortuosity of porous media. As such, our ability to predict effective diffusion coefficients in porous media is inadequate and, additional laboratory work is needed to investigate the impact of the medium itself on transport by diffusion. In addition, experimental data on gas-liquid diffusion coefficients is particularly scarce for tight rocks. This study therefore proposes an experimental methodology, based on the pressure-decay technique, to measure gas-liquid diffusion signals in different rocks to better understand the impact of the rock matrix on the effective transport of fluids by diffusion. The diffusion experiment on the bulk oil (without porous medium) provides an upper limit estimation of gas-liquid diffusion coefficient. The diffusion experiments on limestone and Bakken shale provide insight into different degrees of restriction caused by the medium, captured in terms of effective diffusion. Two analytical models, and one numerical model, were implemented and compared to determine the diffusion coefficients from the time dependent pressure-decay data. These diffusion coefficients agree with the literature, demonstrating the validity of the modeling approaches used. Rock tortuosity and constrictivity were found to affect effective diffusion coefficients, indicating the hindrance effect caused by the pore structure in the rock matrix. By comparing the results from the diffusion experiments with and without the presence of a porous medium, we can assess the restriction caused by the pore network. This is helpful in building more accurate transport models dominated by diffusion, in particular when direct effective diffusion coefficient measurements are scarce.

TABLE OF CONTENTS

LIST OF FIGURES

LIST OF TABLES

ACKNOWLEDGEMENTS

I would like to sincerely thank my advisor Dr. Zuleima T. Karpyn. I am immensely grateful for her endless support, patience and guidance during my entire master study. Words cannot express how grateful I am for her tremendous help.

I would like to thank my entire family for their encouragement and support throughout my life. To my father, Yishan Lou, my mother, Ying Zhang, my grandmother Jiming Zhu, and my grandfather Jiagui Zhang: thank you for everything you have done for me. I never tell you enough how much I love you. I deeply dedicate this work to you.

I would like to thank my girlfriend Siwen Wang for her unconditional help for the experiments, presentations, and writing in this work. Her love encourages me to strive to attain my goals. I love you.

I must thank Dr. Luis F. Ayala for his professional guidance and valuable suggestions in this work. I appreciate his efforts. I cannot accomplish this work without his great help.

I would also like to thank my committee members Dr. Luis F. Ayala and Dr. Hamid Emami-Meybodi for serving on my committee and improving this research. I also appreciate the Hess Corporation and Sandia National Laboratories for the providing support funding for this study

I would like to express my gratitude to my friends Dr. Nirjhor Chakraborty, Dr. Miao Zhang and Dr. Qian Sun for their time and technical help in this research. I learned a lot from them, and they are always my great example to follow. I must thank Timothy Stecko for his critical technical assistance in lab and all amazing ideas he gave to me. I would also like to thank my colleagues at the Center for Quantitative Imaging (CQI) Lab for all ideas you gave me to help me figure out lots of problems.

Last, I would like to thank all my friends in Penn State. You made my work fun and I will never forget the good time in the past two years.

Chapter 1

Introduction

Shale oil and gas are very important unconventional resources in the U.S. which are changing the world's energy, economic, and political situation. In recent years, the massive shale boom demonstrates that domestic shale plays, which include Bakken, Woodford, Barnett, Fayetteville, Eagle Ford, Haynesville and Marcellus, have accounted for almost 90% of U.S. oil production and all gas production growth (EIA, 2014). Among the seven shale plays, the Bakken shale and Eagle Ford contribute nearly 67% of the U.S. oil production (EIA, 2014). The shale oil and gas production increased over time from 2010 to 2019 in the Bakken region and peaked in 2019 (EIA, 2019).

Nowadays, horizontal drilling and hydraulic fracturing technology have been widely applied in shale reservoirs (French, Rodgerson, & Feik, 2014; Jacobs, 2015). Nonetheless, even if the initial recovery is high in these shale reservoirs, the ultimate recovery factor is predicted to be very low, which is nearly 4%-10% of the original oil in place (OOIP), due to the ultra-low matrix permeability of the shale (Alharthy et al., 2018; Hoffman, 2012). Therefore, the enormous untapped resource potential is expected to motivate the investigation and advancement of EOR technology. It is common knowledge that secondary recovery usually can recover 20%-40% of OOIP, and water-flooding is the most traditional secondary recovery method. The shale reservoirs with multiple fractures and low injectivity, however, indicate that the traditional secondary oil recovery technology is not appropriate to improve oil recovery in shale systems (Gamadi et al., 2014).

Tertiary oil recovery technology is an oil field development technology that relies on physical, chemical, and biological technologies to improve oil recovery by changing the properties of fluids or rocks. For many developed and depleted reservoirs, the application of tertiary

production technologies can slow down the decline rate of oil production and maintain a stable production of crude oil. EOR technology generally refers to chemical flooding, thermal recovery, and gas-injection. In recent years, many unconventional oil reservoirs are being investigated to evaluate the viability of EOR methods in tertiary recovery. Among these EOR applications, the interest in the gas-injection EOR method is compelling because this is a widely accepted and effective method to increase the recovery factor by nearly 10%-15% for conventional reservoirs. However, to the best of our knowledge, the gas-injection EOR method has rarely been tried in shale systems (Sheng, 2015).

In order to achieve the feasibility of gas-injection EOR in shale reservoirs or other tight reservoirs, it is critical to understand flow mechanisms in unconventional systems. However, many traditional mechanisms and theory in conventional reservoirs cannot be directly transferred to unconventional systems. Traditional transport models of fluids based on Darcy's law cannot adequately describe fluid transport in unconventional systems because of challenges such as small to extremely-small pores, interference of gas sorption/desorption, solution/exsolution with transport processes, and altered phase behavior due to elevated capillary pressures (Carlson & Mercer, 1991; Ertekin, King, & Schwerer, 2007; Freeman, Moridis, & Blasingame, 2011). One consequence of the extremely small matrix permeability values encountered in ultra-tight formations is that fluid velocities may be so small that diffusion can become the dominant transport mechanism (Amann-Hildenbrand, Ghanizadeh, & Krooss, 2012). Diffusion coefficient, bulk phase diffusion coefficient, or molecular diffusion coefficient refers to a proportionality constant between the molar flux due to molecular diffusion and the gradient in the concentration of the species. Diffusion coefficient is encountered in Fick's law and numerous other equations of physical chemistry. Determination of the diffusion coefficient is important to describe the rate of dynamic mass transfer between injected gas and crude oil in formation (Zhang, Hyndman, & Maini, 2000). Also, the effect of diffusion on gas-injection efficiency has been recognized by various scholars

(Grabanski et al., 2016; Imai, Sumikawa, Yamada, & Nakano, 2012; Rahmanian, Aguilera, & Kantzas, 2013; Ratnakar & Dindoruk, 2015; Yuan et al., 2014). Especially for low-permeability reservoirs with multiple fractures and high capillary pressure, gravity drainage caused by the density difference between the gas and oil is limited. The physical diffusion, similar to gravity, results in the change of the path of the injected gas species from the fractures to the matrix, giving rise to late breakthrough (Hoteit & Firoozabadi, 2006).

In a porous medium, the effective diffusion coefficient decreases compared with the real diffusion coefficient. Standing on the point of fundamental mechanism of diffusion process, this is because the available cross section for diffusion is less than for the bulk fluid and the distance between one point and another in the porous material is less than the distance that a molecule must travel to move between these points. As a result, the normal concentration gradient is greater than the real concentration gradient in porous media. Also, in narrow liquid-filled pores, the order of magnitude of effective diffusion coefficient may be reduced through an increase in drag which in turn is due to a greater viscosity of the solvent (Grathwohl, 2012). This increase in viscosity, compared to the bulk viscosity of the solvent, is caused by the proximity of the pore wall (Cussler, 1984). This is especially applicable to small pores and narrow pore throats which have diameters in the same order of magnitude as the diffusing molecules. Thus, tortuosity and constrictivity are practical properties of rock to explain this steric hindrance effect or restricted diffusion phenomenon. Determining effective diffusion parameters, therefore, is a critical factor for the design of gas-injection in unconventional systems. It is noticeable, however, that reference material on the effective diffusion coefficient is limited, particularly for tight matrix and unconventional fluids. The purpose of this study is to assess the difference of diffusion between bulk fluids and different porous rocks, as well as provide a practical and replicable procedure for estimating diffusion parameters in porous rock.

Chapter 2

Literature Review

2.1 Gas-Injection EOR Technology

The EOR method of gas-injection first appeared in the 1920s. This EOR technology developed quickly when researchers became familiar with the concept of physics and chemistry of multiphase flow through porous media in the early 1950s (Rao, 2001). Gas-injection EOR is presently the most effective approach to enhance oil recovery (Nour, Yaacob, & Alagorni, 2015). Hydrocarbon gas, CO_2, N_2, flue gas, and air can be used in gas-injection EOR technology. This technology encompasses the two main processes of gas-injection: miscible and immiscible oil displacement (Thomas, 2008). In addition, gas-injection generally can be divided into three different modes: gas flooding, huff and puff, and cyclic gas injection. Gas flooding is the injection of hydrocarbon or nonhydrocarbon components into oil reservoirs that are typically waterflooded to residual oil (Johns & Dindoruk, 2013). In the huff and puff EOR process, a well can produce separated gas during the puff period, and it will be injected back in the formation by the same well during the huff period (Sheng, 2015). As long as the produced gas is injected back to the reservoir through either the huff-and-puff mode or gas flooding mode, and this process is repeated, it is cyclic gas injection (Yu, Lashgari, Wu, & Sepehrnoori, 2015).

Concerning the gas-injection modes, gas flooding is inefficient for shale systems. Since natural and artificial fractures often present in shale reservoirs, the fracture network is more complex than it is for conventional reservoirs, resulting in gas channeling that seriously affects the oil displacement (Wan, Sheng, Soliman & Zhang, 2016; Wang & Li, 2019). Furthermore, Zuloaga et al. (2017) point out that the huff and puff cyclic gas-injection method is considered the better

injection mode to overcome low-injectivity in tight reservoirs when the permeability of the reservoir is lower than 0.3mD.

CO_2 huff'n'puff cyclic gas-injection is a popular and highly efficient EOR gas-injection operation (Thomas & Monger, 2007). In this process, CO_2 is injected into an oil reservoir, and then oil and gas can be mixed in any proportion and all mixtures remain in a single phase. There is no interface between the fluids due to the single phase, therefore, no interfacial tension, which minimizes the remaining oil saturation (Teletzke, Patel, & Chen, 2005). At the same time, the concept of relative permeability does not apply since there is no distinct phase. Further, the relative wettability of the rock to the oil and the injected fluid are not influencing factors. Miscible displacement is equivalent in oil-wet and water-wet rocks, which can greatly improve the oil recovery. Thus, the main mechanism of gas-injection EOR is using gas to lower the gas/oil interfacial tension. Also, reducing oil viscosity and density can lead to increased mobilization of oil and oil swelling.

The minimum miscible pressure is a significant factor for characterizing the miscible process in reservoirs, but it is not the only parameter for the design of the gas-injection EOR technique (Wang & Li, 2018). This is because fluids transport in the porous media of shales and coals are increasingly controlled by molecular diffusion rather than convection flow (Han et al., 2010). Also, the Peclet number (Pe) corresponding to laboratory (Pe~1000) MMP measurements can be substantially greater than those encountered in reservoir settings with Pe ~100 for conventional reservoirs and Pe < 0.1 for unconventional reservoirs. During the oil recovery process in low-permeability reservoirs that used the gas-injection or thermal solvent injection technique, a mass transfer phenomenon occurs when gas and oil come into contact. Mass transfer is a prior condition for diffusion, and it is affected by molecular structures and surface activity (Kovaleva, Davletbaev, Babadagli, & Stepanova, 2011). With more and more injected gas diffusing in the reservoir, it can break through the convection front zone. Lower gas/oil interfacial tension and

reduced oil viscosity can improve the flow ability of fluids to enhance oil recovery. In addition, molecular diffusion allows the gas to penetrate through the crude oil, thereby inhibiting viscous fingering, delaying early gas breakthrough and increasing oil production (Bardon & Denoyelle, 2012).

As mentioned above, determining and accurately measuring the solubility of gas in the oil and diffusion coefficients are the keys evaluating the feasibility of miscible gas flooding. In addition, molecular diffusion is a critical parameter in the reservoir simulation models to capture real flow mechanisms when gas is introduced to a tight oil system (Yu, Lashgari, & Sepehrnoori, 2014).

2.2 Experimental Measurement of Diffusion Parameters

Diffusion parameters mainly include the diffusion coefficient and solubility. The diffusion coefficient, also known as diffusivity, is the proportional constant between the molar flux caused by molecular diffusion and the concentration gradient. Diffusion can be described by Fick's law and many other physical and chemical equations (Liu et al., 2016). In the petroleum engineering field, the measurement of gas-liquid diffusion coefficients in the laboratory usually requires the measurement of mass transfer parameters. But the determination of mass transfer characteristics relies on sophisticated technology and experimental instruments to measure the concentration of a specific area and the related parameters. Experimental methods for determining the diffusion coefficient can be classified into direct methods and indirect methods. The principle of direct methods is the analysis of the change in the composition of the diffusion species over time (Schmidt, 1982). The common direct methods are mass spectrometry (Mikkelsen, 1982), radio-active tracer technique (Marlowe & Kaznoff, 1968), and spectrophotometry (Simpliciano et al., 2013). These methods can extract the profile of concentration of a specie as a function of diffusing

distance for estimating the diffusion coefficient. However, the direct measurements are time-consuming, costly, and highly susceptible to experimental errors (Upreti & Mehrotra, 2002).

In theory, indirect methods can measure any change of a characteristic of tested fluids caused by the diffusion process. The main indirect methods are Nuclear Magnetic Resonance (NMR), Computed Tomography (CT) Analysis, and Pressure Decay (PD). The NMR method is based on the principle that the variation of the NMR spectrum caused by the change of the mixture property in the diffusion process can determine the diffusion coefficient, which is related to the concentration and rate of mass transfer (Taylor & Bushell, 1985). X-ray CT imaging can measure the density change in a specific area of the system and then convert the system density into mass concentration and volume concentration through the corresponding formula, and finally determine the diffusion coefficient through Fick's law (Nakashima, 2000). From above review, there are many mature technologies for measuring diffusion coefficient in bulk fluids (Wen, Kantzas, & Wang, 2010). It is noticeable, however, that adapting it to porous media has been a challenge, especially for unconventional porous rocks.

The pressure-decay method is more practical in the laboratory for porous rocks (Yang, Dong, Gong, & Li, 2017). The modified pressure-decay method is based on a closed system with constant pressure and temperature. Since the diffusivity is a function of the partial pressure of the gas, the diffusivity can be obtained from the data of pressure decline over time. The pressure-decay method is widely used in bulk fluids and porous rocks for its convenient operation, simple steps, and accurate results (Creux et al., 2005; Etminan, Maini, Chen, & Hassanzadeh, 2010; Ghaderi, Tabatabaie, Hassanzadeh, & Pooladi-Darvish, 2011; Jamialahmadi, Emadi, & Müller-Steinhagen, 2006; Li & Yang, 2015; Riazi, 1996; Sheikha, Pooladi-Darvish, & Mehrotra, 2005; Tharanivasan, Yang, & Gu, 2006; Zhang et al., 2000).

2.3 Pressure-Decay Techniques

The earliest measurements of diffusion coefficients of gas in liquid hydrocarbons were performed by Pomeroy et al. (1933) by measuring the quantities of methane dissolved in oil under constant gas pressure as a function of time. However, difficulties in the maintenance of constant pressures, and accurate measurements of gas absorption volumes were some of the challenges of this approach. The modern pressure decay method introduced by Riazi (1996) uses the transient pressure fall-off data for a closed gas-oil system to infer diffusion coefficients. In a closed pressure vessel, the final state of the system depends on thermodynamic equilibrium after unsteady gas and liquid contact. At the gas-liquid interface, the thermodynamic mechanical equilibrium between the two phases always exists. Also, the position of the interface and the pressure of the system both are functions of time. The position and pressure of the gas-liquid interface depend on the diffusion rate of species from one phase to another. Diffusion rate also refers to the diffusion coefficient. Therefore, Riazi (1996) proposed a semi-analytical model to predict the mass transfer rate caused by the diffusion between the gas and the liquid under the condition of high pressure and constant temperature in a closed system. The pressure and interface position calculated by the model are consistent with the experimental results, which verifies the reliability of the model. Zhang et al. (2000) developed a simple pressure-decay method based on the study from Riazi (1996). In this method, a model combining the diffusion equation with the gas material balance equation was used. The diffusion coefficient was used as an adjustable parameter to conduct the history matching of the gas absorption data. Tharanivasan et al. (2004) found that diffusion coefficient was very sensitive to interface boundary conditions by using the model from Zhang et al. (2000). They also believed that reasonable selection of interface boundary conditions would directly affect the interpretation quality of experimental data. Furthermore, several models considered other factors such as resistance to mass transfer at the interface (Brenner & Leal, 1978), swelling of oil (Luo,

Kryuchkov, & Kantzas, 2007) and equilibrium boundary conditions (Civan & Maurice, 2001; Civan & Rasmussen, 2002).

Sheikha et al. (2005) presented a new analytical model assuming that the bottom of the pressure cell was an infinite-acting boundary. This is a first inversion graphical method based on the analytical solution for estimating gas-liquid diffusion parameters. Etminan et al. (2009) designed a new modified pressure-decay experiment that maintains constant concentration at the gas-liquid interface and measures the amount of gas transferred to the liquid as a function of time. Pacheco and Hejazi (2015) proposed a new approximate analytical solution of pressure profile by using the integral method. Based on previous studies, Ratnakar and Dindoruk (2015, 2016, 2018) used the Laplace transform technique to obtain an exact solution for estimating the diffusion coefficient and equilibrium concentration. Therefore, the determination of diffusion parameters of gas in the bulk liquid phase by the pressure-decay method has been extensively studied. This current study will implement analytical models from Pacheco and Hejazi (2015) and Ratnakar and Dindoruk (2015) for estimating the diffusion coefficient and equilibrium constant of gas in bulk liquid .

However, a consequence of the difficulty of measuring the gas-liquid diffusion coefficient in porous media in the laboratory has led to relatively few research studies. Renner (1988) developed a novel experimental approach and corresponding mathematical model for measuring diffusivity of CO_2 in liquid-saturated consolidated cores by using the pressure-decay technique. Li and Dong (2009) proposed a new numerical model for radial diffusion, which can also provide a tool for studying the diffusion of CO_2 in liquid-saturated porous rocks at a high pressure in the lab. This new method was improved from Riazi (1996), it was unnecessary to measure the change of gas-liquid interface with time. Thus, the oil-swelling effect can be negligible in this method. Through the simultaneous diffusion equation and gas balance equation, the relation curve between gas pressure and time is fitted, and then the diffusion coefficient can be obtained through the

variable parameters obtained by fitting. Yang et al. (2017) proposed an experiment and the matching analytical solution, which considered the non-equilibrium boundary condition, to match with the entire pressure-decay experimental process of solubility and diffusion coefficient of methane in oil-saturated unconsolidated porous media. Zhang et al. (2019) proposed a straightforward numerical model for free gas phase and adsorbed gas phase transport in shale nano-pores. The results indicate that adsorption/desorption is a non-equilibrium process during gas transport in shale, and this process can be accurately modeled using sorption model of kinetics. This research will apply this numerical model for evaluating diffusion parameters of methane in oil-saturated porous rocks.

Chapter 3

Research Objectives

Based on a review of literature on the current state of knowledge on diffusion mass transport and gas-injection EOR in tight reservoirs, the main objectives of this work have been defined as follows:

1. To develop an experimental methodology to measure effective diffusion in porous media.

As mentioned in Chapter 2 Literature Review, there are currently no well-established methods to measure effective diffusion coefficients in porous materials. Estimation of diffusion coefficients is best done through direct measurement approaches such as mass spectroscopy, radioactive tracers, spectrophotometry, or any other experimental modality wherein the diffusing components are measured directly over time. However, such methods are expensive, time-consuming, and often extremely challenging to design in lab. The pressure-decay technique, an indirect approach, is widely applied to measure diffusion of gas in bulk liquid phase. But there is still no mature pressure-decay experimental setup and protocol for porous media. The purpose of this research is to propose a modified experimental methodology to accurately measure gas-liquid diffusion parameters in porous rocks.

2. To implement and compare modeling approaches for estimating diffusion parameters.

It is essential to determine diffusion parameters. However, only pressure-decay data can be obtained from experimentation. A modeling approach is required to interpret experimental data and extract diffusion parameters. Although some modeling approaches are proposed by previous studies, there is a lack of additional literature to verify their methods. Also, the

shortcomings of some methods should be analyzed. Thus, not only should the modeling method be implemented, but different modeling approaches should be compared with each other, and the results should be compared with published data.

3. To assess the sensitivity of the gas-liquid effective diffusion coefficients in different porous rocks, and attempt to correlate the diffusion coefficient and the effective diffusion coefficient based on molecular diffusion theory.

Lab measurements of diffusion coefficients are often performed on bulk fluids without accountability for the restricted diffusion caused by the geometric complexity of porous media. The tortuosity and constrictivity factor are properties of rocks accounting for this steric hindrance effect. However, it is hard to measure these properties of rocks, resulting in the difficulty in correlating the diffusion coefficient to the effective diffusion coefficient. In addition, limited research provide insight into the effect of properties of different rocks on effective diffusion coefficients. In order to better understand the knowledge in this area, this study therefore attempts to assess the sensitivity of the gas-liquid effective diffusion coefficients in different porous rocks, and to estimate tortuosity in different porous rocks for correlating the diffusion coefficient and the effective diffusion coefficient.

Chapter 4

Methodology

4.1 Experimental Methodology

The modified pressure-decay experiments were performed to quantify the diffusion of methane in Bakken oil under the two different scenarios: bulk liquid phase and porous rocks. The difficulty of the modified pressure-decay experiment is to capture the clear pressure-decay data. In particular, the clear pressure-decay signal is hard to be acquired in the rock sample with extremely small pore volumes. Figure 4-1 indicates that the larger gas to oil volume ratios (Vg/Vo) at the start of the experiment can lead to smaller total pressure drop by equilibrium. The lower ratio of the gas volume to the oil volume, the greater pressure fall-off signal can be obtained. The reason is that the transducer records the change of gas cap pressure, if the gas volume is too large, the signal of the changes of pressure shows very weak. Even if the diffusion process happens in the pressure cell, it is hard to observe it through the corresponding pressure-decay data. This reduces the reliability of the data and can make the subsequent modeling process challenging.

For bulk liquid phase, the gas volume is the volume of gas in the gas cap, and the oil volume is the volume of the oil that partially filled with the pressure cell. For porous media, the gas volume is nearly equal to the dead volume in annulus and flowlines, and the oil volume is nearly equal to the pore volume of the rock sample. Therefore, the technical problem of the modified pressure-decay experiment in lab is the difficulty in controlling the ratio of the gas volume to the oil volume for porous rocks with limited pore volume. In order to acquire a clear pressure-decay signal, the rule from Figure 4-1 should be followed, and an appropriate ratio of gas volume to oil volume should be achieved in each experiment.

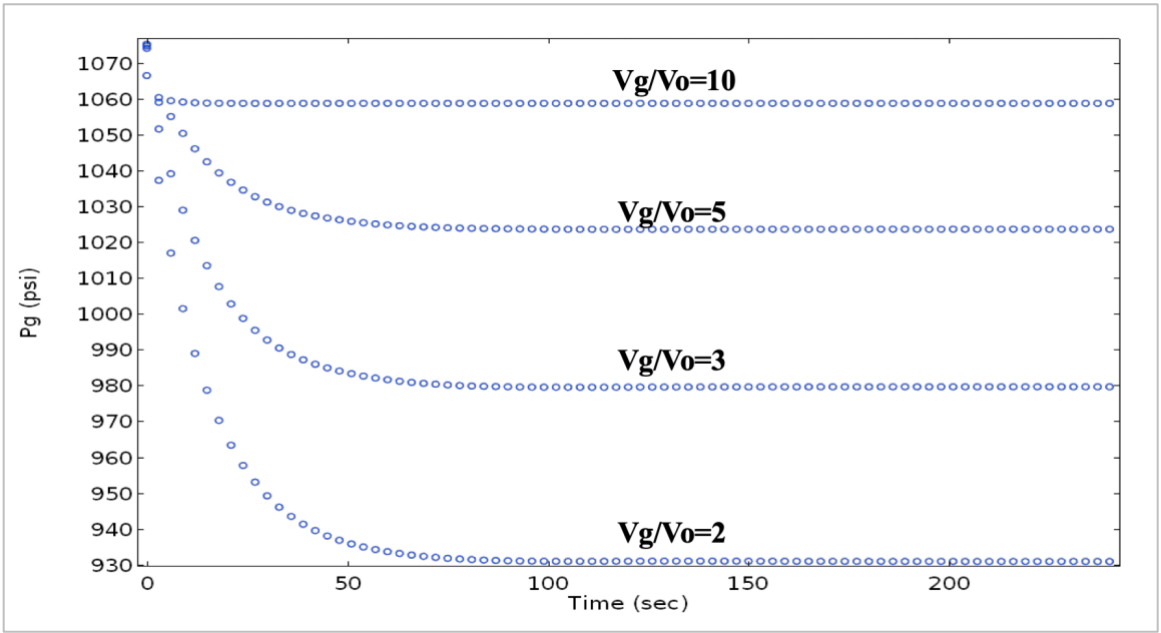

Figure 4-1: Relation between the pressure-decay signal and ratio of gas volume to oil volume

4.1.1 Materials

In this study, for all experiments, methane with a purity of 99.97% is chosen as the probe gas, and the liquid is produced oil from Bakken shale reservoir. This choice is done for following reasons: First of all, methane and shale oil are live gas-liquid systems in shale systems, indicating it is of more practical significance for the research. Accurate prediction of diffusion coefficients of methane in liquid hydrocarbons is one of the key parameters for improving the prediction of compositional oil reservoir simulators, for designing surface facilities, and for high pressure gas/liquid mass transfer operations (Jamialahmadi et al., 2006). In addition, methane is a common gas for solvent-based recovery processes, but the experimental data of methane is relatively less than that of carbon dioxide and inert gas. Conducting experiments on methane can fill the void of the limitation of the experimental data.

Two types of rocks are used in diffusion tests. The reason for this is to study the effect of rocks with different complexity of pore structures on the restricted diffusion. Indiana limestone is

a second test case between the bulk fluids and Bakken shale. It can provide some hindrance effect on the diffusion, but also has the relatively simple pore structure for Bakken shale. The specific properties of limestone are listed in Table 4-1.

Table 4-1: Physical characteristics of Indiana limestone (Kojadinovich, 2018)

Property	Values	Units
Length	20	cm
Diameter	5	cm
Effective porosity	15-18	%
Absolute Brine Permeability	100-250	mD

The Bakken shale samples are provided from the Hess Corporation. Every Bakken shale sample is 0.45-inch diameter, and 1.3-inches length cylindrical plugs. In order to increase the pore volume for capturing diffusion signal, three samples were used in a single test. The porosity of the Bakken shale cores was measured via helium porosimetry and found to be around 8%, while permeability was estimated in the low micro Darcy range.

4.1.2 Experimental Apparatus

(1) Methane diffusion in bulk oil

A pressure decay experiment was performed on methane and Bakken oil by using a high-pressure reactor vessel. The diameter and height of this vessel are 6.2 cm and 21 cm, respectively. There are five ports on the vessel cap, but only two are connected parts on the top cap, and the rest are sealed by plugs. One of the two ports connect the Quartzdyne digital pressure transducer, which can measure up to 10000 psi. The other port connects a main high-pressure valve that can introduce gas or depressurize gas. Gas can be introduced into the pressure vessel through the high-pressure

valve connecting gas cylinder. During the experimental process, the pressure will reach two pressure stages of 1000 psi and 2000 psi. The reason is that this operation is helpful to control the pressure more easily, and the results con provide a comparison about the decay data at different pressure stages. A certain amount of oil (543.43 cm^3) occupying 60% of the vessel is placed in the vessel, and it can make the ratio of the gas volume to the oil volume 1:6, which is small enough (obey the rule from Figure 4-1) to detect the diffusion signal from the pressure-decay data. The whole system is placed in a temperature-controller water bath to maintain the room temperature. The schematic of experimental set-up is shown below in Figure 4-2.

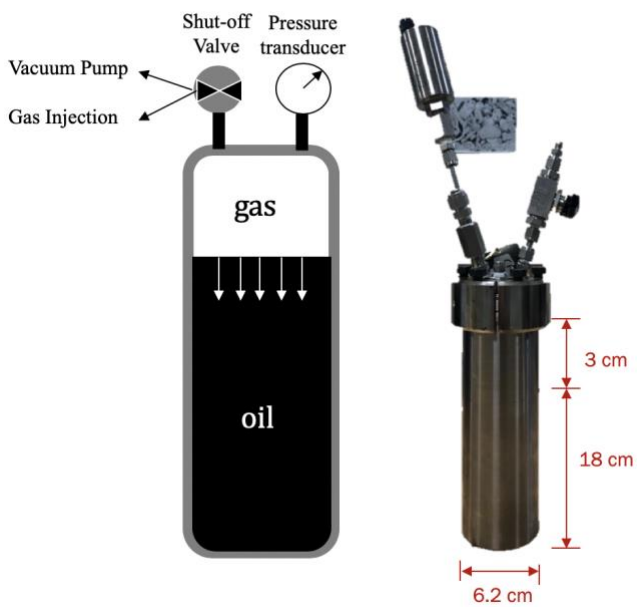

Figure 4-2: Schematic of the experimental setup and actual experimental apparatus for bulk fluids

(2) Methane diffusion in oil-saturated limestone

The limestone is chosen as the second test case between bulk fluids and Bakken shale. Figure 4-3 shows the schematic and actual experimental apparatus of this experiment, which was

similar to that of the bulk fluids experiment. Because the dimension of limestone is large, the ratio of the gas volume to the oil volume can be achieved as 2:1. In addition, for all diffusion experiments on the porous rocks, the two ends of the cylindrical core plug are sealed. Thus, methane can only penetrate the cylindrical core plug through the radial direction, which works for the modeling purpose in the next part.

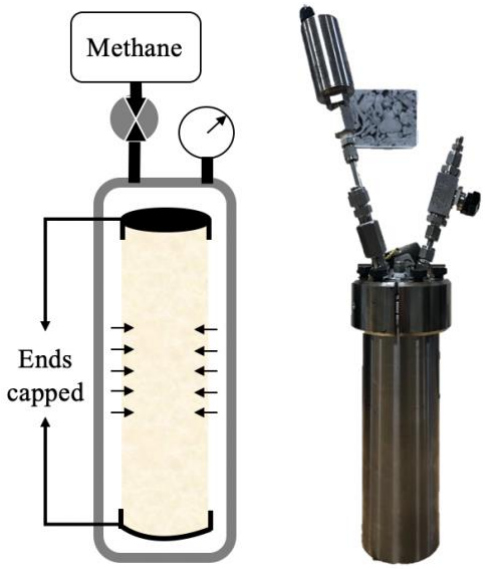

Figure 4-3: Schematic of the experimental setup and actual experimental apparatus for limestone

(3) Methane diffusion in oil-saturated Bakken shale

In this work, the diffusion experiment on Bakken shale can be conducted by using the special designed pressure vessel. This new pressure vessel is better suited to the dimension of Bakken shale. It has two ports, one end of which is directly connected to the Omega digital transducer and the other end is connected to the 1/16-inch valve. Note that all the designs of this system are trying to reduce gas volume as much as possible by minimizing the dead volume in annulus and flowlines, thereby resulting in a system that is more sensitive to the change of pressure. Thus, this is a more appropriate system for the rocks with more complex geometric pore structure.

The ratio of the gas volume to the oil volume is 3:1. The schematic of experimental set-up is shown below in Figure 4-4.

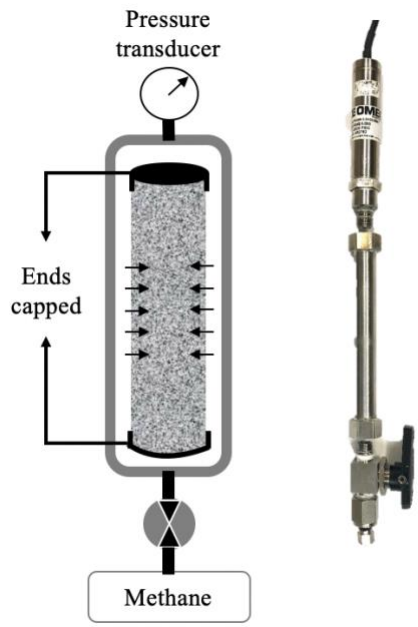

Figure 4-4: Schematic of the experimental setup, and actual experimental apparatus custom designed and constructed for Bakken Shale experiment

4.1.3 Experimental Procedure

(1) Methane diffusion in bulk oil

First, the empty vessel was pressurized with the test gas for a leak test at approximate 2000 psi. The pressure drop in 3 days was less than 4 psi (0.06%/day), which is within the tolerance of 0.1%/day. Next, the vessel was depressurized to get ready for the experiment. Then, the pressure vessel was partially filled with Bakken oil to achieve the desired volume of the oil and then the whole system was vacuumed for 24 hours to minimize the air in the experimental setup. After that, the valve on the top of the vessel was opened, methane was introduced at a 2000 psi resulting in an instantaneous buildup of pressure. The pressure shock that comes with the gas injection equilibrate instantaneously and oil is nearly incompressible. Last, shut off the inlet valve and methane started

to diffuse in bulk Bakken oil. During the process of the pressure-decay experiment, the pressure fall-off profile was recorded by the digital pressure transducer. The experimental setup was placed in the temperature-controller water bath to maintain the temperature.

(2) Methane diffusion in oil-saturated limestone

The experimental setup was pressurized with the test gas for leak test at approximate 2000 psi to make sure the pressure change in 3 days was less than 4 psi (0.06%/day), which is within the tolerance of 0.1%/day. Then, prepared the limestone that was heated and vacuum dried. Next, sealed the two ends of the fully oil-saturated limestone and placed the limestone sample in the pressure vessel. After performing the short evacuation of the dead volume for minimizing air, introducing methane at 1000 psi and instantaneous buildup of pressure. Shut off the inlet valve and pressure falloff were recorded till stabilization. After the whole system stabilized, increased pressure to 2000 psi stage and monitored pressure decline. The experimental setup was also placed in the temperature-controller water bath to maintain the temperature.

(3) Methane diffusion in oil-saturated Bakken shale

The experimental procedure to measure the pressure falloff in Bakken shale was conducted. It is a similar procedure to that of the limestone. First, tested the sealing ability of the empty special designed pressure at 2000 psi. When the pressure drop was less than 0.06%/day, the system was ready for the formal experiment. Next, the Bakken samples were heated and vacuum dried. Then, the samples were fully saturated with Bakken oil and placed in the new pressure vessel. Note that for modeling purpose, the all ends of samples were also capped for forcing gas to penetrate sample through radial direction. After a short evacuation of the dead volume for minimizing air, introducing methane at 1000 psi and instantaneous buildup of pressure. Next, the inlet valve was closed, and pressure falloff was recorded till stabilization. After that, the 2000 psi stage was able to be obtained. Similarly, the experimental vessel was placed in the water bath to control the temperature.

4.2 Modeling Methodology

Three different methods are introduced in this section. Table 4-2 displays all methods and applied conditions.

Table 4-2: An overview for Modeling Approaches

Methods	Condition
A Graphical Approach (Pacheco & Hejazi, 2015)	Bulk Liquid
A Simplified Graphical Approach	Bulk Liquid
Numerical Modeling	Bulk Liquid & Porous Media

As indicated by Pacheco and Hejazi (2015), a graphical approach can be executed for the condition of the gas diffusion in bulk liquid phase for 1D cartesian. This method can use late-time pressure-decay data from previous experimental methodology to estimate the diffusion coefficient and Henry's constant of the gas in the oil. Due to the basis of the 1-D transient diffusion model in the vertical direction, this method can be implemented only for the condition of gas diffusion in bulk liquid. Next, a simplified graphical approach is developed based on Ratnakar and Dindoruk (2015). It is still for gas diffusion in bulk liquid condition; however, a simplified integral method is used to shorten the calculation steps and simplify the whole process. As for the numerical model, it was proposed by our research group in COMSOL. The pressure fall-off data from the condition of the gas diffusion in the bulk oil or oil-saturated porous media can be analyzed. The detailed procedures are shown below.

4.2.1 A Graphical Approach

Figure 4-5 depicts the phenomena of gas diffusion in bulk oil in a pressure cell. When gas is introduced from the top, it will start to diffuse in the bulk oil vertically in this closed system. In this schematic, h_G is the height of the gas cap and h_L is the height of oil column.

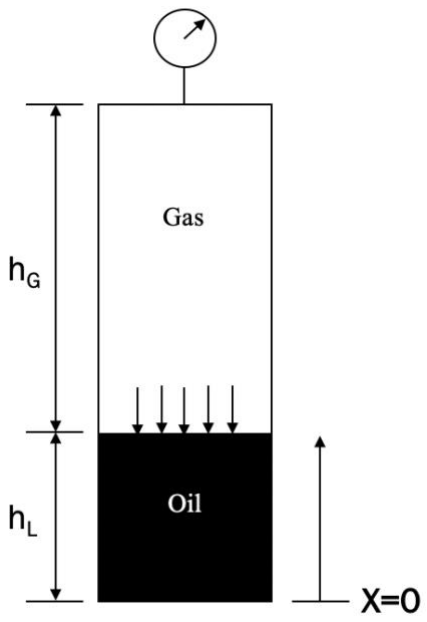

Figure 4-5: Schematic of pressure-decay cell

Based on previous studies (Sheikha et al., 2005), the following assumptions should be considered in this diffusion model:

1) Constant volume system;

2) Isothermal system;

3) Constant diffusion coefficient and gas-compressibility factor;

4) No chemical reaction between the gas and liquid;

5) Swelling effect of liquid is negligible;

6) At the gas/liquid interface, there is no resistance to mass transfer and the interface should obey the mass balance equation;

7) The concentration of the gas component in the gas phase is assumed to be uniform because the diffusion transport in the gas phase is very fast. Also, gas is introduced into liquid from top following x-direction, so the transverse concentration gradient can be ignored.

After the illustration of assumption, the diffusion process can be mathematically described by Fick's second law.

$$\frac{\partial C}{\partial t} = D\frac{\partial^2 C}{\partial x^2} \tag{4-1}$$

where C is the concentration of the gas in the oil phase, t is the transition time, D is the diffusion coefficient, and x is the height from the pressure cell bottom.

The initial condition is given below, indicating the concentration of gas in the oil phase is zero at the beginning of the experiment:

$$C(t = 0, x \leq h_L) = 0 \tag{4-2}$$

Henry's law is a gas law that states that the amount of dissolved gas in liquid is proportional to its partial pressure above the liquid (Henry, 1803). In addition, the rate of gas dissolving into the bulk oil should be equal to the rate of gas leaving the gas cap. Thus, the boundary condition can be obtained as below:

$$P = H_{ij}C \tag{4-3}$$

$$\mathrm{DA}(\frac{\partial C}{\partial X})_{X=h_L,t>0} = (\frac{V_g M}{ZRT})\frac{dP}{dt} \tag{4-4}$$

where P is the gas cap pressure, H_{ij} is the Henry's constant, D is the diffusion coefficient, A is the cross-sectional area of the gas/oil interface, V_g is the gas volume (V_g=Ah_G), M is the molar weight of gas, Z is the gas-compressibility factor, R is the universal gas constant, and T is the temperature.

Also, by substituting equation (4-3) into equation (4-4):

$$(\frac{\partial C}{\partial t})_{x=0} = \psi \frac{H_{ij}}{D} \frac{dC}{dt} \tag{4-5}$$

where ψ is given by the following equation:

$$\psi = \frac{h_L M}{ZRT} \tag{4-6}$$

Assuming there is no-flow in the bottom of the pressure cell due to the closed system, the bottom boundary condition is as follows:

$$(\frac{\partial C}{\partial t})_{x=h_L} = 0 \tag{4-7}$$

In order to solve equation (4-1), based on the boundary and initial conditions from equations (4-2), (4-5), (4-7), an approximate analytical late-time solution, which can predict measurements of pressure as a function of time, is presented by using the integral method:

$$P(t) = \frac{P_o}{1 + \frac{h_L}{\psi H_{ij}}} \left\{ 1 + \frac{h_L}{\psi H_{ij}} exp \left[-\frac{12}{5} \frac{(1 + \frac{h_L}{\psi H_{ij}})}{\frac{{h_L}^2}{D}} t \right] \right\} \tag{4-8}$$

where P_o is the initial pressure.

According to equation (4-8), the diffusion coefficient and Henry's constant can be calculated by the following steps:

Step1: Determining the early-time and late-time regime from pressure fall-off data is the first step. Each diffusion process under the above simulated conditions can be divided into early-time and late-time regime. On the one hand, early-time regime begins when the pressure cell is pressurized and gas molecules start to diffusion in bulk oil, and it terminates when gas molecules penetrate the oil body and reach the bottom of the pressure cell. On the other hand, late-time regime starts after the moment of gas molecules reach the bottom of the pressure cell, and it terminates when the system reaches equilibrium. For the analytical model, the late-time model can be used to

calculate diffusion parameters from the late-time regime data. Thus, the following equation is selected to acquire experimental late-time pressure decay data:

$$\mathrm{erfc}^{-1}\left[\frac{P(t)}{P_o}\right] = \frac{\sqrt{D}}{\psi H_{ij}}\sqrt{t} \tag{4-9}$$

This early-transient time equation suggests a straight line for the experimental data related to the early-time regime by plotting the pressure-decay data in the form of $\mathrm{erfc}^{-1}\left[\frac{P(t)}{P_o}\right]$ as a function of $\sqrt{t}$. It is also important to note that for this method, the experimental data is required to be smoothed before implementation; otherwise, the real experimental data cannot be analyzed.

Step 2: For the convenience of calculation, let:

$$r_1 = \frac{P_o}{1 + \frac{h_L}{\psi H_{ij}}} \tag{4-10}$$

$$r_2 = \frac{h_L}{\psi H_{ij}} \tag{4-11}$$

$$m_1 = \frac{12}{5}\frac{(1 + \frac{h_L}{\psi H_{ij}})}{\frac{{h_L}^2}{D}} \tag{4-12}$$

Thus, equation (4-8) can be simplified as follows:

$$P(t) = r_1 + r_1 r_2 exp(-m_1 t) \tag{4-13}$$

Then, by taking the logarithm of both sides of the equation (4-13), the following equation can be derived:

$$ln\left[-\frac{1}{P_o}\frac{dP(t)}{dt}\right] = -m_1 t + ln(r_1 r_2 m_1) \tag{4-14}$$

This equation suggests that a plot of $\ln\left[-\frac{1}{P_o}\frac{dP(t)}{dt}\right]$ vs. t should be first a straight line for which the slope is m_1. m_1 is a very important parameter for calculating the diffusion coefficient and Henry's constant.

Step 3: Substitute known m_1 to into equation (4-13), and then the second straight line can be obtained by plotting P(t) vs. exp(-m_1t). The intercept (b_1) for this straight line can be known.

Step 4: After acquiring m_1 and b_1, Henry's constant and diffusion coefficient can be calculated by the following equations:

$$H_{ij} = \frac{h_L}{\psi}\left(\frac{b_1}{P_o - b_1}\right) \tag{4-15}$$

$$D = -\frac{5}{12}\frac{m_1 {h_L}^2}{\left(1 + \frac{h_L}{\psi H_{ij}}\right)} \tag{4-16}$$

The flow chart is shown below:

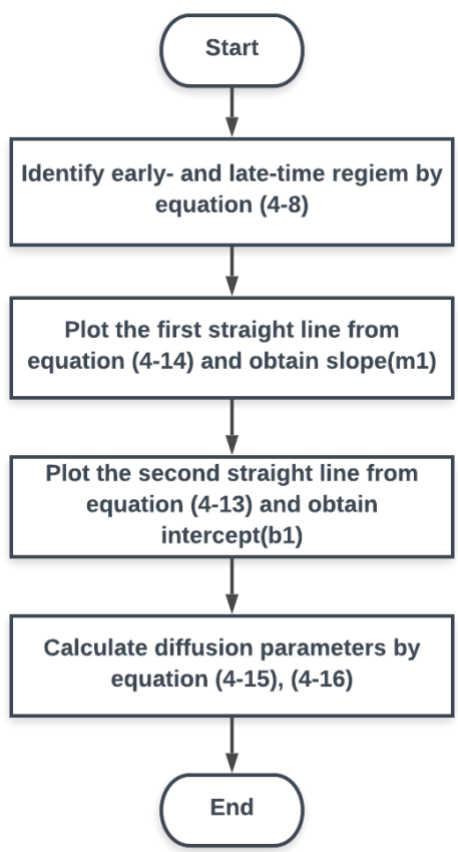

Figure 4-6: Flow chart for the graphical approach (Pacheco & Hejazi, 2015)

4.2.2 A Simplified Graphical Approach

This simplified graphical approach was developed based on previous studies (Ratnakar & Dindoruk, 2015, 2016, 2018). This simplified graphical approach and the above graphical approach (Pacheco & Hejazi, 2015) have the same assumptions. The process of diffusion can also be described as the mathematical equation (4-1). Initial conditions are shown as below:

$$\rho_g = \rho_{go} = \frac{P_o}{Z_o RT} \tag{4-17}$$

$$C(t = 0, x \leq h_L) = 0 \tag{4-18}$$

where ρ_g is gas molar density, ρ_{go} is initial gas molar density, Z_o is the gas-compressibility at initial pressure and temperature. The standing katz chart is a widely accepted technique for estimating real gas compressibility, but evaluating the Z factor from reading the chart will lead to an inaccurate value. Dranchuk and Abu-Kassem's (1975) method is employed for calculating gas-compressibility.

The interface condition and boundary condition are shown as follows:

$$DA(\frac{\partial C}{\partial X})_{X=h_L, t>0} = -\frac{d(V_g \rho_g)}{dt} \tag{4-19}$$

$$K_H = \frac{C_{go,int}(t)}{C_{gg}} \tag{4-20}$$

$$(\frac{\partial C}{\partial t})_{x=h_L} = 0 \tag{4-21}$$

where $C_{go,int}$ is the concentration of the gas component in the oil phase dependent upon pressure and C_{gg} is the concentration of the gas component in the gas phase. Equation (4-19) is another form of equation (4-4) in which P is substituted by ρ_g. Equation (4-20) is another form of Henry's law. Henry's constant here is dimensionless, and the relation between H_{ij} and K_H is shown below:

$$K_H = \left(\frac{L}{\psi}\right) H_{ij} \tag{4-22}$$

The detailed derivation process can be found in Appendix A.

Ratnakar and Dindoruk, (2015) used the Laplace-transform method to develop an exact analytical solution for the molar density of gas:

$$\frac{\rho_g(t) - \rho_{g\infty}}{\rho_{go}} = \sum_{i=1} \frac{2}{(1 + \alpha K_H + \frac{\lambda_i^2}{\alpha K_H})} exp(\frac{-\lambda_i^2 Dt}{h_L^2}) \tag{4-23}$$

where α is the ratio of gas volume and oil volume, $\rho_{g\infty}$ is the equilibrium gas molar density, and λ_i are the roots of following equation:

$$tan(\lambda_i) = -\frac{\lambda_i}{\alpha K_H}; \lambda_i \neq 0, i > 0 \tag{4-24}$$

Note that equation (8) is an approximate solution purposed by implementing the integral method for solving equation (1). The concentration of gas (C) is approximate as a cubic polynomial, indicating the truncated solution and approximate results. In contrast, equation (23) is a completed solution developed by Laplace transform which is more accurate.

If only the first root of equation (4-24) is dominant, and equation (4-23) can be simplified as following equation:

$$\rho_g(t) = \rho_{g\infty} + \beta \exp(-m_2 t), t > t_{tr} \geq \frac{1}{3m_2} \tag{4-25}$$

$$m_2 = (\frac{-{\lambda_1}^2 D}{{h_L}^2}) \tag{4-26}$$

$$\beta = \frac{2\rho_{go}}{(1 + \alpha K_H + \frac{{\lambda_1}^2}{\alpha K_H})} \tag{4-27}$$

where β is the rate coefficient of pressure decay, m_2 is the exponent factor that determines the rate of pressure decline, and t_{tr} is the transition time, which represents the beginning of the late-time regime.

Based on the equation (4-23), the following steps can be implemented to calculate the diffusion coefficient and Henry's constant:

The first step is to select the experimental late-time regime data. Only the late-time regime data can be analyzed by late-time solution, so the first point *t* selected from the experimental data should be t_{tr}. At the beginning, equation (4-9) can be used to quickly predict t_{tr}. Note that this approach doesn't require the smoothed data, so the experimental data can be implemented directly. The experiment also doesn't need to be completed, but limited data may result in significant error.

Then, the equation (28) shows a simplified intergral solution based on equation (4-25).

$$\frac{1}{\rho(t)-\rho_{t_f}}\int_t^{t_f}\rho(t)dt=\rho_{g\infty}\left[\frac{t_f-t}{\rho(t)-\rho_{t_f}}\right]+\frac{1}{m_2} \tag{4-28}$$

where ρ_{t_f} is the last point of the molar density from the experimental data points, t_f is the last point of time from the experimental data points, and ρ_∞ is the predicted equilibrium molar density for the experiment. Through this equation, $\frac{1}{\rho(t)-\rho_{t_f}}\int_t^{t_f}\rho(t)dt$ vs. $\frac{t_f-t}{\rho(t)-\rho_{t_f}}$ can be plotted to obtain intercept ($\frac{1}{m_2}$) and slope (ρ_∞). The detailed derivation can be seen in Appendix A.

Next, diffusion coefficient and Henry's constant can be calculated by the following equations:

$$D=\frac{1}{{\lambda_1}^2}{h_L}^2 m_2 \tag{4-29}$$

$$K_H=\frac{\rho_{go}-\rho_{g\infty}}{\alpha\rho_{g\infty}} \tag{4-30}$$

Last, check the values that the t is larger than $\frac{1}{3m_2}$, and if so, the results can be accepted. On the contrary, experimental data points should be added or subtracted from the original analyzed pressure-decay data.

The main flow chart for this simplified graphical approach is shown below:

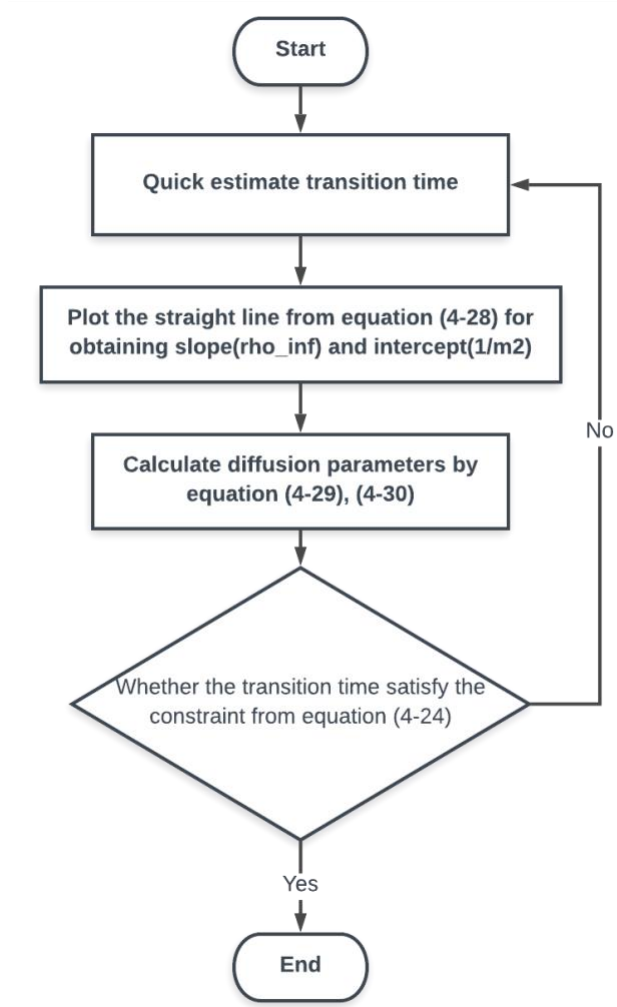

Figure 4-7: Flow chart for the simplified graphical approach

4.2.3 Numerical Modeling

Following the study of Zhang et al., (2019), the general reservoir transport equation for any multicomponent, multiphase system, can be expressed as the following:

$$\frac{\partial(\phi C_{IJ})}{\partial t} - \nabla\left[\left(\phi D_{IJ} + \frac{k}{\mu_J c_J}\right)\nabla C_{IJ}\right] = R_{IJ}, I = 1,2,\dots,N_c, I = 1,2,\dots,N_c \quad (4\text{-}31)$$

where ϕ is the porosity of the porous media, C is the concentration of the I component in J phase, D_{IJ} is the effective diffusion coefficient of component I in phase J, k is the absolute permeability

of the porous media, μ is the viscosity, c_J is real gas compressibility, and R_{IJ} is the interphase mass exchange of component I into/out of phase J.

For diffusion-dominated transport, and in single-phase oil, two-component (gas/oil) system, $R_{IJ} = 0$, the diffusion-only RTE becomes:

$$\frac{\partial}{\partial t}(\phi C) = \nabla(\phi D_{Io} \nabla C) \tag{4-32}$$

Neglecting porosity (or for clear fluid cases), for the gas component (I=G) and a constant diffusion coefficient system, it is written in terms of molar concentrations as follows:

$$\frac{\partial C_{Go}}{\partial t} = \nabla(D_{Go} \nabla C_{Go}) \tag{4-33}$$

(1) The gas diffusion in the bulk oil

The modeling approach presented here follows the results of Riazi, Whitson, and Silva, (1994). The pressure cell remains at constant volume and temperature conditions. Figure 4-8 depicts the boundary conditions during the diffusion process in the pressure cell.

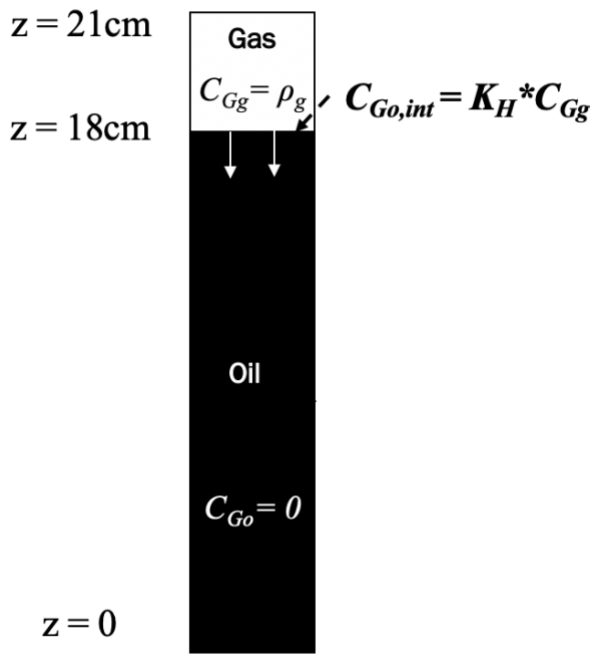

Figure 4-8: Numerical model for bulk oil experiment

Considering diffusion in the vertical direction (z-direction) only, for the system shown in Figure 4-8, the initial condition is:

$$C_{Go}(t = 0, z) = 0 \tag{4-34}$$

The bottom of the cell is sealed. Thus, this boundary condition is:

$$\frac{\partial C_{GO}}{\partial z}(\mathrm{z} = 0, \mathrm{t}) = 0 \tag{4-35}$$

At the interface, gas and oil are assumed to be at equilibrium, and gas is assumed to travel in the oil as a dissolved species. Henry's law therefore applies,

$$C_{GO}(z = L_o, t) = K_H C_{Gg}(z = L_o, t) = K_H \rho_g(P) \tag{4-36}$$

where K_H is the Henry's constant, ρ_G is the gas phase density, and P is the pressure of the cell.

The output of the model is the gas cap pressure, which is assumed to be uniform.

$$C_{Gg}(z = L_o, t) = C_{Gg}(P_{gas-cap}) = \rho_G(P_{gas-cap}) \tag{4-37}$$

where $P_{gas\text{-}cap}$ is the gas cap pressure.

Thus, the gas transport equation in bulk oil can be shown as below:

$$\frac{\partial}{\partial z}(D_{GO}\frac{\partial C_{GO}}{\partial z}) = \frac{\partial C_{GO}}{\partial t} \tag{4-38}$$

(2) The gas diffusion in the oil-saturated cylindrical porous rocks

In order to match the experiment, the geometry of this model has been changed. Gas can penetrate only the oil-saturated core through the radial direction as shown in Figure 4-9.

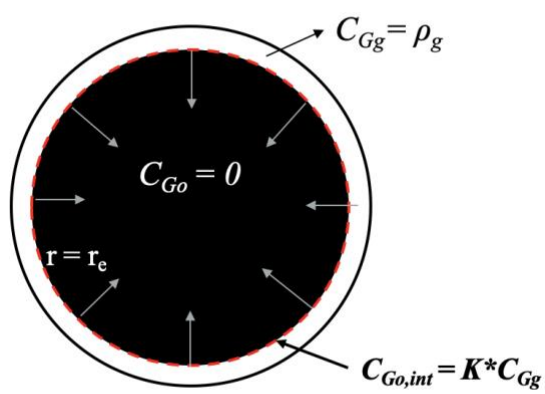

Figure 4-9: Numerical model for porous media experiments

The porous media model is an adaptation of the clear fluids model for a porous medium 100% saturated with oil and for 1D radial transport.

$$\phi\frac{\partial C_{GO}}{\partial t} = \nabla(\phi D_{Go}\nabla C_{GO}) \tag{4-39}$$

The output of the model is the annular gas pressure, which is assumed to be uniform.

$$C_{Gg}(r = r_e) = C_{Gg}(P_{annular}) = \rho_G\left(P_{gas-cap}\right) \tag{4-40}$$

Where $P_{annular}$ is the gas pressure in annulus, r_e is the radius of cylindrical core plug, and r_a is the radius of pressure cell.

Thus, the gas transport equation in oil-saturated porous media can be shown as below:

$$\frac{1}{r}\frac{\partial}{\partial r}(\phi D_{GO} r \frac{\partial C_{GO}}{\partial r}) = \phi \frac{\partial C_{GO}}{\partial t} \tag{4-41}$$

Chapter 5

Results and Discussion

5.1 Experimental Pressure-Decay Data

As stated in Chapter 4.1 Experimental Methodology, during every single test, the pressure-decay is recorded by the pressure transducer. There are four tests presented in this part, and every experimental pressure-decay plot conforms to an exponential decay behavior. It is a curve of pressure over time, and a change in the slope at each point on the curve represents the velocity of the gas diffusing through the liquid. The faster the pressure declines, the faster the gas diffuses in bulk liquid. At the same time, the greater the pressure drop is, the more mass of the gas is dissolved in the liquid.

Figure 5-1 shows the result of the experimental gas pressure decay data of methane diffusion in bulk oil starting from a methane injection pressure of 1689 psi. The time span of this experiment was 75 days during which equilibrium was not reached, thus, there is no clear pressure plateau to be observed. It is noted that the fluctuations in the measured decline pressure data are due to the ± 2 psi variance in the pressure measurement accuracy at any given time. In addition, for modeling approaches, a clear exponential pressure decay signal is captured, indicated by the pressure fall-off (~600 psi).

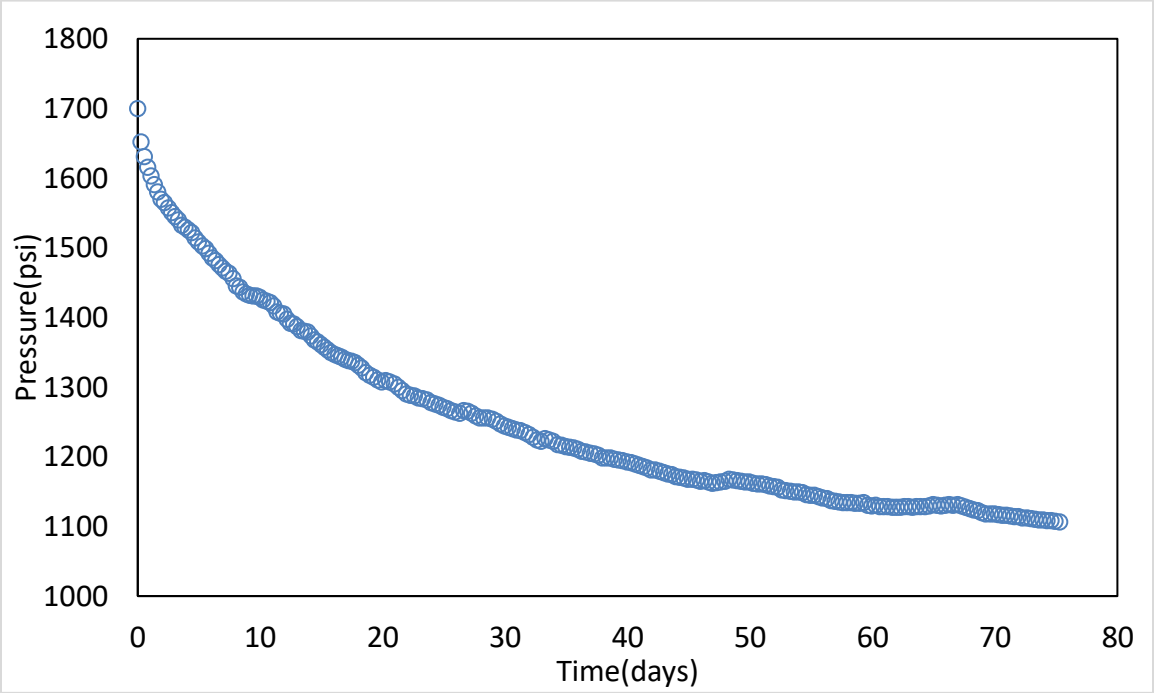

Figure 5-1: Experimental pressure-decay during methane diffusion in bulk oil at P_o=1689 psi – error: ±2 psi

The results of tests on porous media are displayed from Figure 5-2 to Figure 5-4. The experimental result of the pressure decay data acquired from measurements on the oil-saturated limestone core is shown in Figure 5-2. To start, pressure equilibrium was achieved within 20 days. The pressure drop is nearly 60 psi and the pressure fluctuations are less than 2 psi, indicating that the pressure fluctuation is only 0.1% of pressure drop scale. Then, based on this stabilized condition, pressure was increased to a higher stage (1848 psi) as shown in Figure 5-3.

Figure 5-3 displays the result of the experiment referred as gas diffusion oil-saturated limestone with higher pressure. This is because at the end of the prior stage (Figure 5-2), the pressure had been increased. After the experimental pressure increased, the equilibrium time was shortened to 7 days, and the pressure drop became nearly 50 psi, indicating the rate of diffusion became faster with pressure. Also, pressure fluctuations are less than 0.3 psi, which is acceptable.

The experimental results of the pressure decay data acquired from measurements on the stacked oil-saturated Bakken core are exhibited in Figure 5-4. Pressure equilibrium was achieved within 7 days, and the pressure drop is nearly 50 psi. Similarly, acceptable pressure fluctuations (±3 psi, 0.3%) were obtained in this experiment.

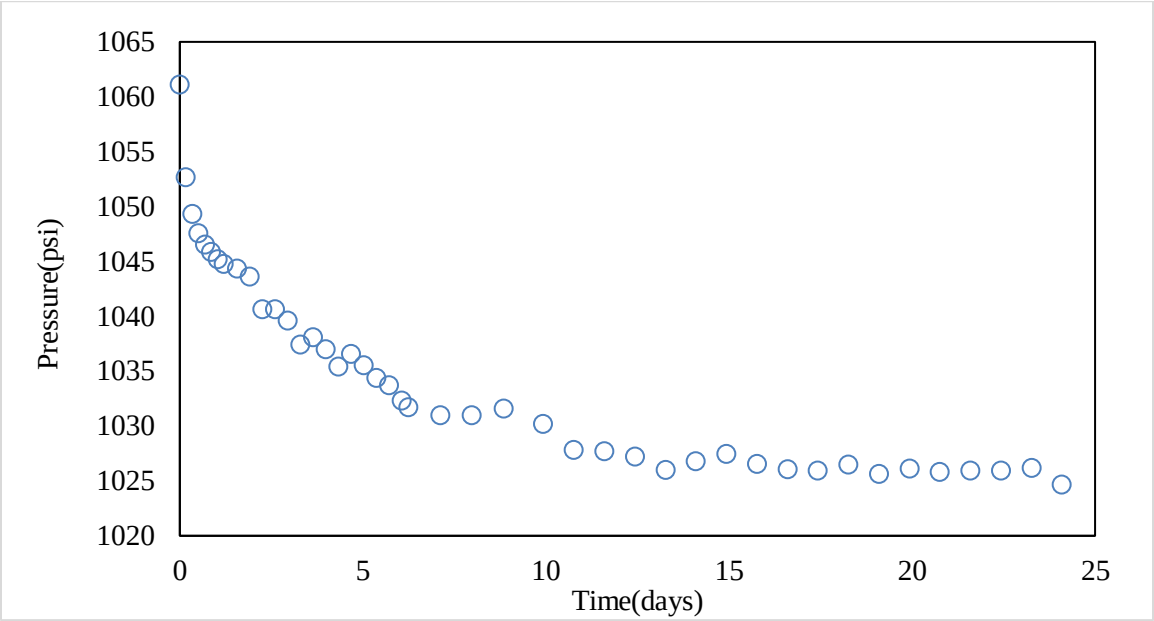

Figure 5-2: Experimental pressure-decay during methane diffusion in oil-saturated limestone at P_o=1061 psi – error: ±2 psi

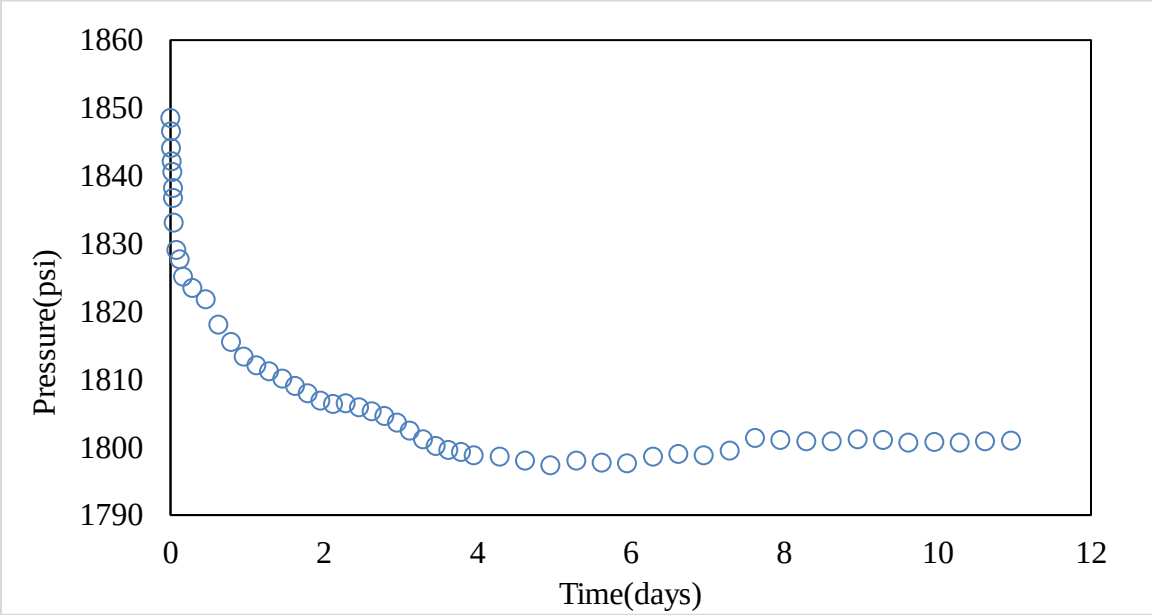

Figure 5-3: Experimental pressure-decay during methane diffusion in oil-saturated limestone at P_o=1848 psi – error: ±2 psi

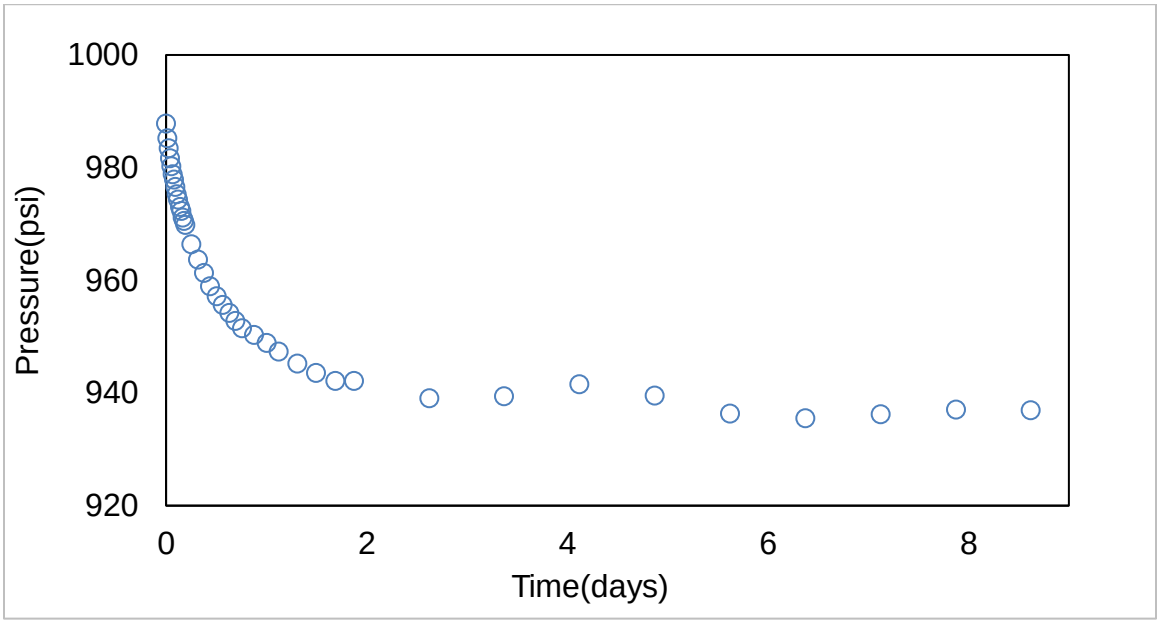

Figure 5-4: Experimental pressure-decay during methane diffusion in oil-saturated Bakken shale at P_o=987 psi – error: ±5 psi

In order to make the pressure-decay signal measurable, a small gas volume should be achieved in the experiment. This will make the system very sensitive to the fluctuation of internal and external changes of the environment during the experiment. Although there are pressure fluctuations in the experimental results, the fluctuations are within the error range of the transducers. Besides the error of the pressure transducer, this phenomenon may be explained by following possible reasons: The pressure cells were placed in a laboratory with a constant temperature, but the temperature difference between day and night could slightly affect the pressure; The gas-liquid interface in the pressure cell could not be detected in the experiment. When the gas diffused in the liquid phase, the liquid volume might expand, causing the gas-liquid interface to move; In the process of moving or checking the experimental setup, the vibration of the system could affect the pressure decay system.

5.2 Estimated Diffusion Parameters in Bulk Oil

5.2.1 Graphical Approach

The first graphical approach results are shown as the following:

Figure 5-5 delineated the plot from equation (4-9) for the smoothed experimental data of methane diffusion in bulk oil. On the basis of Figure 5-5, the early-time and late-time regime can be separated. The experimental data in the early-time regime is on a straight line, and rest of the data that deviates from the straight line in the late-time regime can be observed. Thus, the late-time regime of the experiment started at nearly 256 hours for this case.

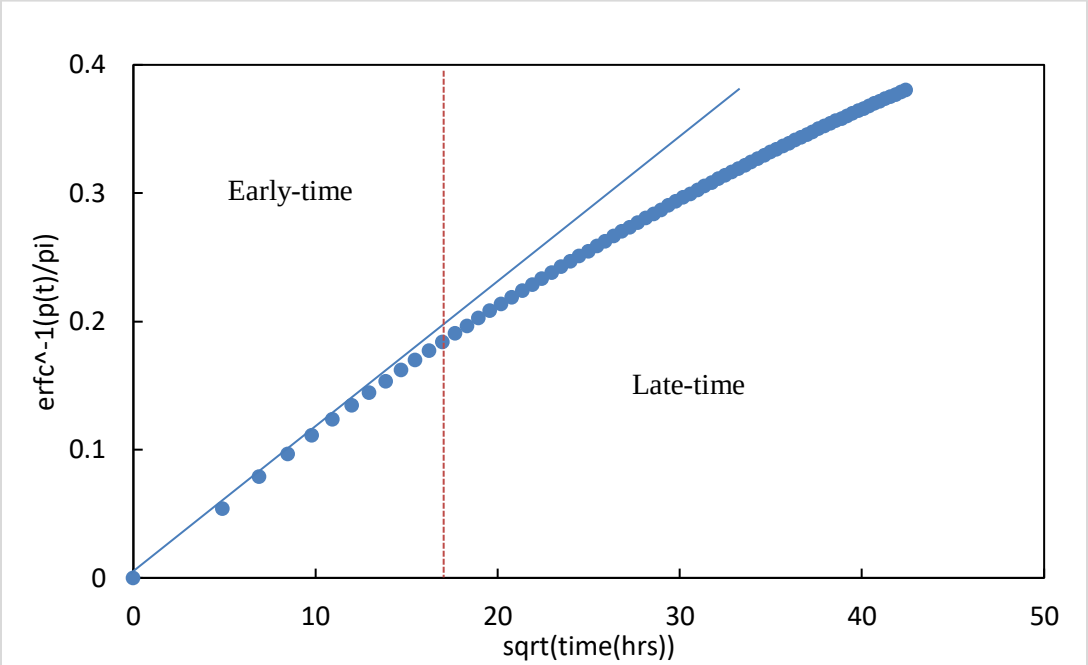

Figure 5-5: Partition of the pressure-decay data corresponding to the early- and late-time regime - methane diffusion in bulk oil

After identifying the early-time and late-time regime of the experimental pressure-decay data, the first straight line belonging to this method can be obtained based on equation (4-14) displayed in Figure 5-6. According to the regression function, the slope of this straight line is $2.249 \times 10^{-7} s^{-1}$. Also, the plot of the second straight line is presented in Figure 5-7. Based on equation (4-13), the intercept b_1 (863.3 Pa) can be extracted from this straight line. After acquiring these two important parameters, the diffusion coefficient and Henry's constant for this methane diffusion in bulk oil case can be calculated by equation (4-15) and (4-16) from this graphical approach. Thus, the results of the diffusion coefficient and Henry's constant from this graphical approach are $2.09 \times 10^{-9} m^2/s$ and 0.45, respectively.

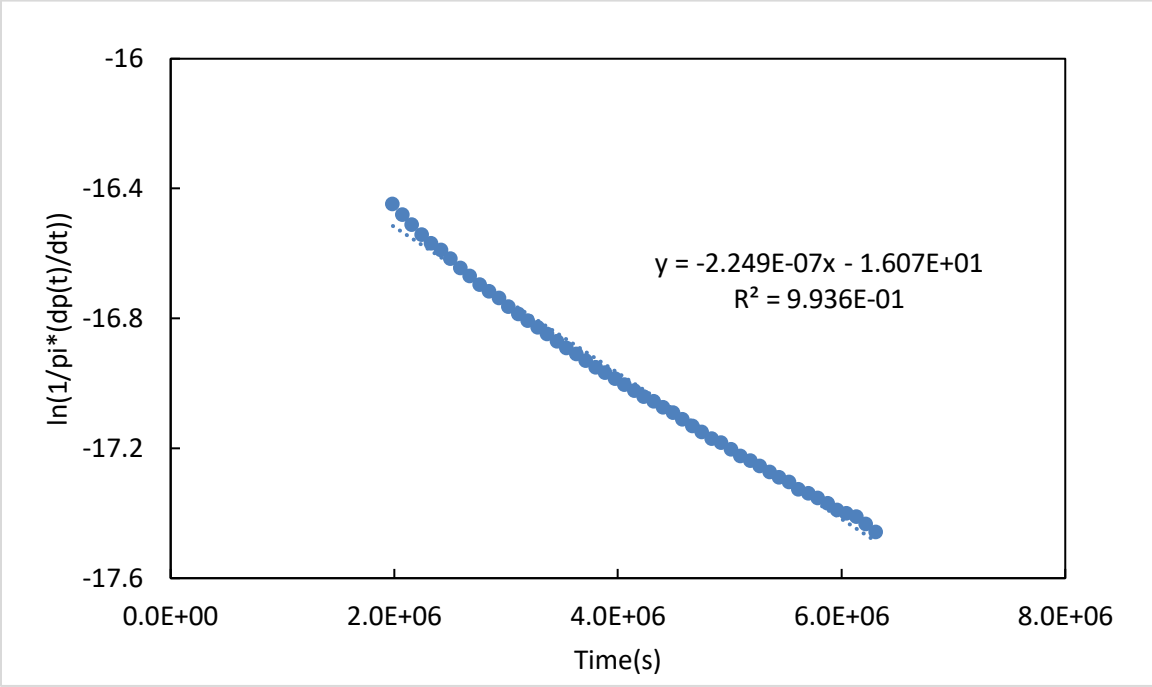

Figure 5-6: The first straight line obtained from equation (4-14)

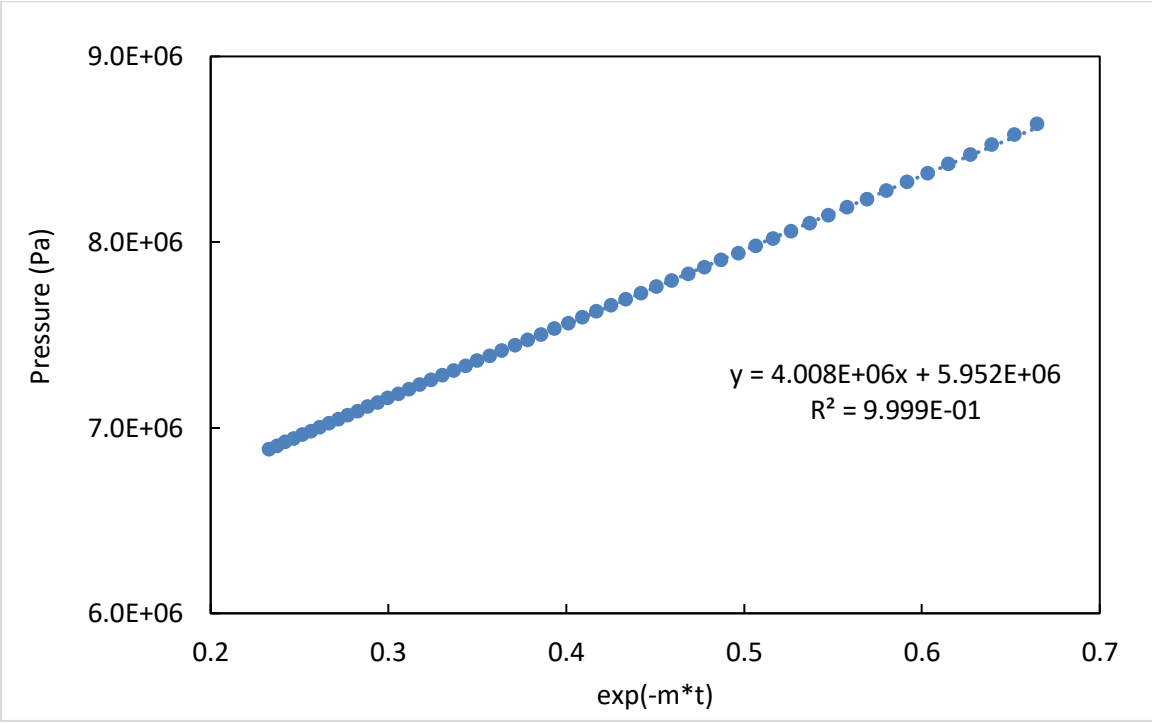

Figure 5-7: The second straight line obtained from equation (4-13)

Based on the slope and the intercept extracted from Figure 5-6 and Figure 5-7, respectively, parameters from this approach can be calculated. Table 5-1 displays these parameters:

Table 5-1: Estimated parameters obtained from the graphical approach

Parameters	**Values**	**Units**
h_L	0.18	m
h_G	0.03	m
R	8.314	$\frac{\mathrm{m}^3 \cdot \mathrm{Pa}}{\mathrm{K} \cdot \mathrm{mol}}$
T	294.261	K
M	16.04	$\mathrm{g/mol}$
Z	0.9	0.9
ψ	2.02×10^{-4}	$\frac{\mathrm{g}}{\mathrm{m}^2 \cdot \mathrm{Pa}}$
H_{ij}	1830.925	$\frac{\mathrm{m}^3 \cdot \mathrm{Pa}}{\mathrm{g}}$
D	2.09×10^{-9}	$\mathrm{m/s}^2$
K_H	0.45	-
m_1	2.25×10^{-7}	s^{-1}
b_1	5.95×10^{-6}	$-$

After the diffusion parameters are obtained, the late-time solution from equation (4-8) can be applied. Figure 5-8 shows the results of the prediction of the experimental data by using the late-time solution. In theory, the late-time solution should match the late-time experimental data after 256 hours; however, there are still differences that cannot be negligible between the fitting data and the experimental data. There are many factors that can lead to inaccurate results such as 1) This is an approximate late-time solution rather than an exact late-time solution; 2) Gas-compressibility is

assumed a constant; 3) The way of smoothing experimental data is different, leading to inaccurate results; 4) Experimental data is not sufficient that cannot cover the full exponential decay.

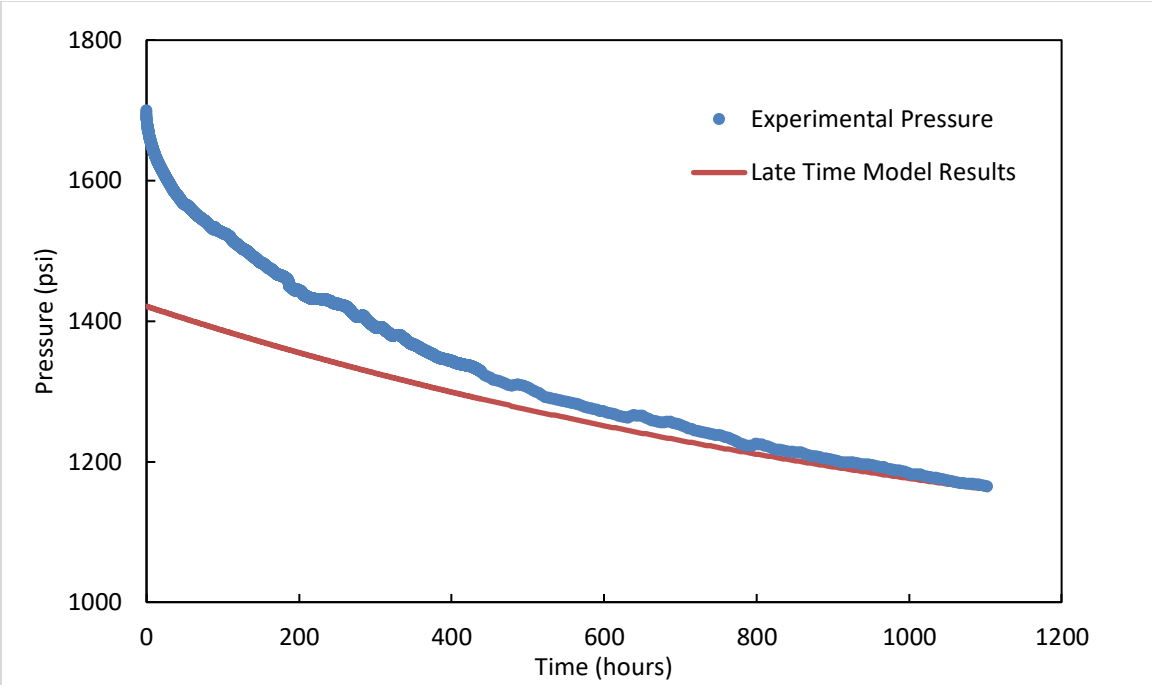

Figure 5-8: Late-time model predictions from graphical approach against experimental data - methane diffusion in bulk oil

5.2.2 Simplified Graphical Approach

Figure 5-9 demonstrates the plot of a straight line based on equation (4-28). According to the regression function, the equilibrium molar density, which is slope equal to 3506mol/L and intercept of this equation equal to 571.4 h^{-1}, can be obtained. Equation (4-39) and (4-30) can be used to calculate diffusion parameters; therefore, the estimated measured diffusion coefficient is $4.35 \times 10^{-9}\ m^2/s$, and Henry's constant is 0.17.

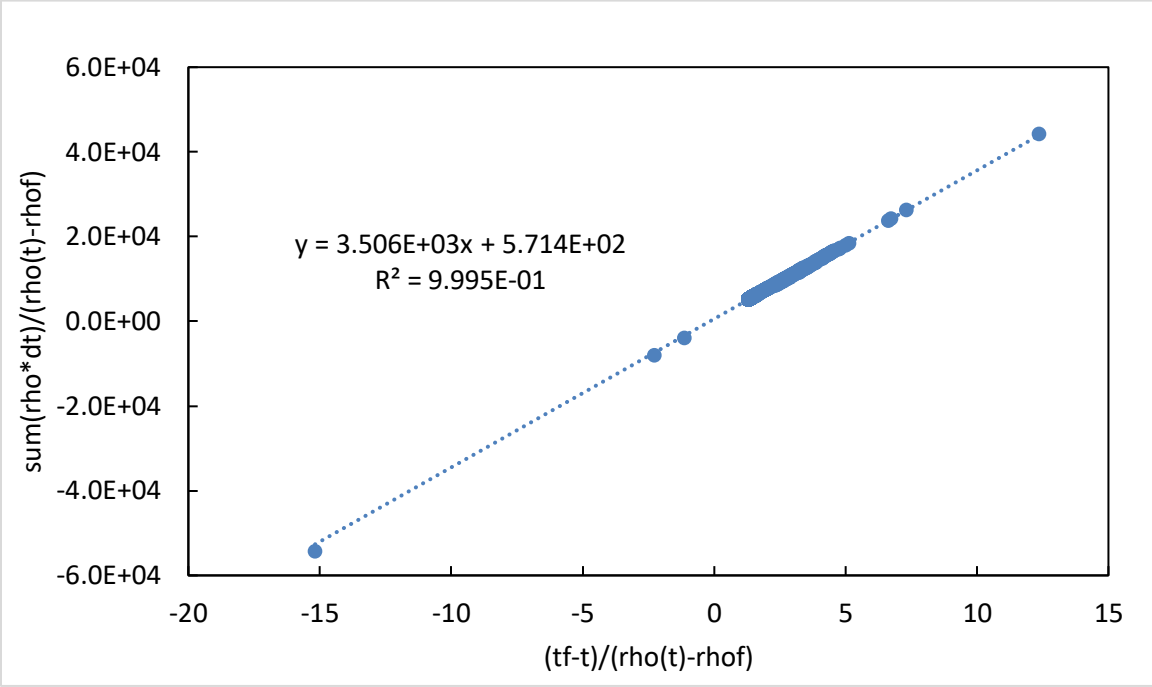

Figure 5-9: The straight line from simplified graphical approach obtained from equation (4-28)

After obtaining Figure 5-9, the intercept and the slope of this straight line can be estimated. Based on known parameters, more needed parameter can be calculated. Table 5-2 lists the calculated parameters:

Table 5-2: Estimated parameters from the simplified graphical approach

Parameters	**Values**	**Units**
h_L	0.18	m
h_G	0.03	m
α	6	-
$\rho_{g\infty}$	3506.211	mol/L
$1/m_2$	571.372	hour
m_2	0.0018	hour^{-1}
t_{tr}	190.457	hour

λ_1	1.902	-
$1/{\lambda_1}^2$	0.276	-
D	1.57×10^{-5}	$\mathrm{m/h^2}$
D	4.35×10^{-9}	$\mathrm{m/s^2}$
K_H	0.109	-
β	1620.627	mol/L

Figure 5-10 indicates the comparison between model results and experimental pressure decay data. The early-time model (green dash curve) can fit the experimental data in the beginning of the experiment. As for late-time solution (red curve), it is roughly able to predict experimental data in late-time regime. Notice that this approach implements real experimental data, which has direct fluctuations, leading to the inevitable error.

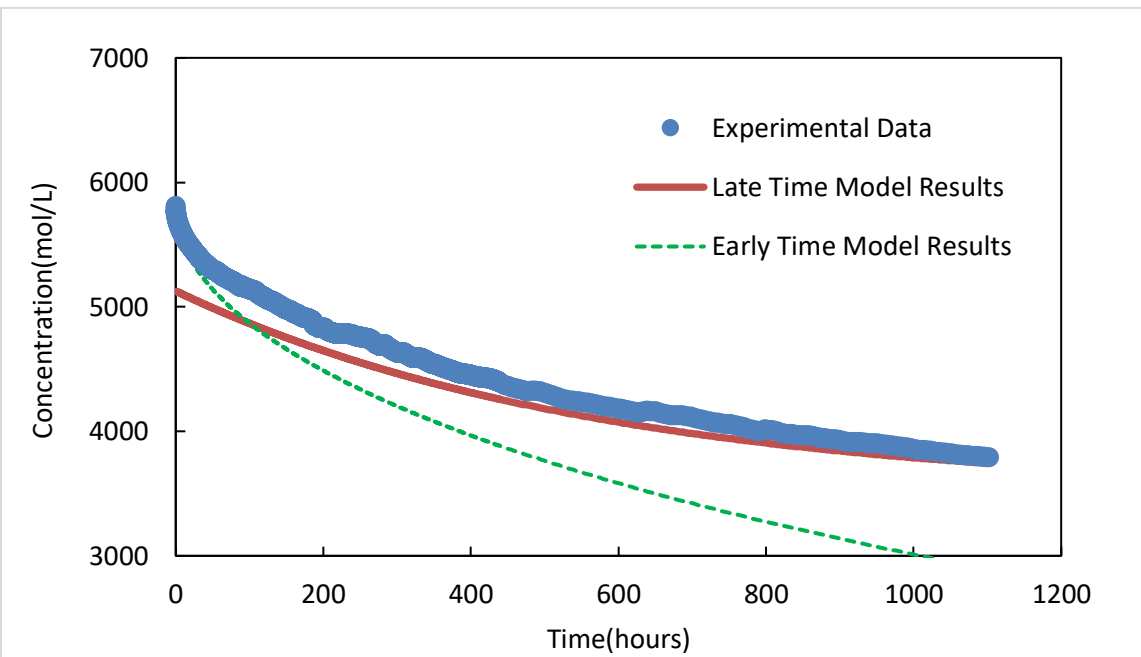

Figure 5-10: Early-time and Late-time model predictions from the simplified graphical approach against experimental data - methane diffusion in bulk oil

5.2.3 Numerical Modeling

In this part, the numerical modeling is applied to estimate diffusion parameters under the condition of methane diffusion in bulk Bakken oil.

First, Figure 5-11 describes the results of history matching for the condition of methane diffusion in the bulk oil, which corresponds to the two previous two analytical models. The experimental data can be divided two parts. The first part of experimental data collected the changes of pressure in 75 days starting from the beginning of the experiment. The second part of experimental data were verified equilibrium pressure data after the system was stabilized. It is not necessary to keep recording the experimental data because the pressure-decay process lasts very long time. Equilibrium density was determined nearly 250 days after the start of the experiment. Therefore, the diffusion coefficient and Henry's constant can be determined as $3.8 \times 10^{-9} \mathrm{m}^2/\mathrm{s}$ and 0.11, respectively. Equilibrium was predicted to be reached in around 150 days.

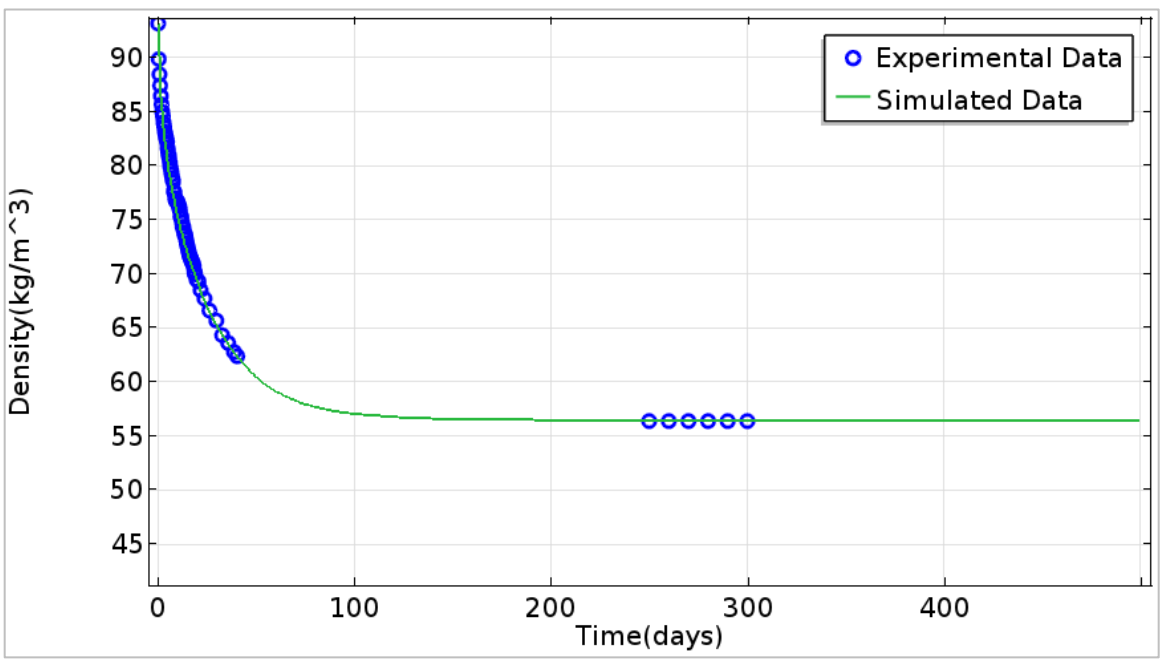

Figure 5-11: History matching of numerical model - methane diffusion in bulk oil

So far, the pressure decay experiment for methane diffusion in bulk oil was implemented by three modeling methods, and different results of diffusion parameters were obtained. The comparison of the three methods is shown in Figure 5-12, and the overall results of the analysis are provided in Table 5-3.

Figure 5-12 summarized the fitting results for the three methods: numerical model has the best match with experimental data, and the two graphical approaches can also predict late-time pressure-decay data. The simplified graphical method is closer to the real data than the normal graphical approach, indicating the simplified graphical method is not only simpler, but also more accurate. In addition, the results obtained by the two graphical methods are within the range of the numerical simulation results, illustrating all measured results are reasonable, and the methods are reliable to implement.

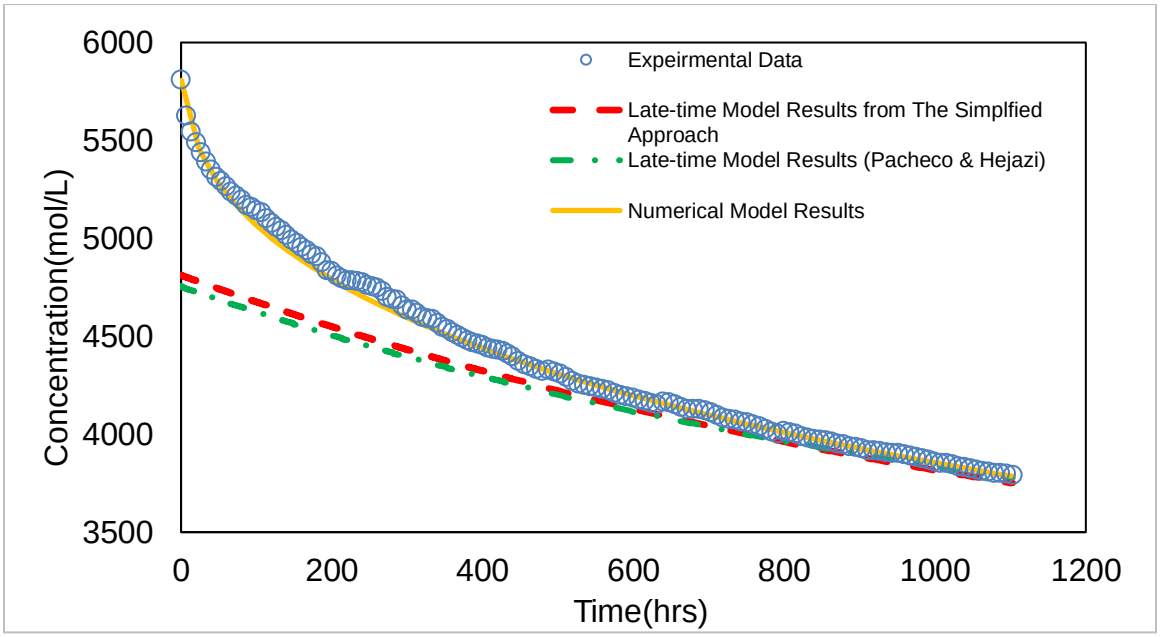

Figure 5-12: The comparison among results of three modeling approaches - methane diffusion in bulk oil

Table 5-3: Diffusion coefficients and Henry's constant for three methods

Methods	Diffusion Coefficient (m^2/s)	Henry's Constant (dimensionless)
Graphical Method (Pacheco & Hejazi, 2015)	2.09×10^{-9}	0.45
Simplified Graphical Method	4.35×10^{-9}	0.17
Numerical Model	3.80×10^{-9}	0.11

Table 5-4 lists some published diffusion parameters. The range of measured diffusion coefficient is from $2.09 \times 10^{-9} \mathrm{m}^2/\mathrm{s}$ to $4.35 \times 10^{-9} \mathrm{m}^2/\mathrm{s}$, which is in agreement with the reference (from $5.2 \times 10^{-11} \mathrm{m}^2/\mathrm{s}$ to $9.8 \times 10^{-9} \mathrm{m}^2/\mathrm{s}$). The range of diffusion coefficients from literature is very wide, indicated by the values differing by two orders of magnitude. This because these experiments were carried out under different gas-oil systems and different experimental conditions. For instance, The diffusion coefficient of the solute gas in the liquid hydrocarbons increases as operating pressure and temperature increase (Jamialahmadi et al., 2006). The solute gas diffuses faster in light oil than heavy oil, indicated by the higher diffusion coefficient (Zhang, Sun, Duan, & Li, 2015). In available literature, Henry's constant is scarce and is relatively limited, illustrating the direct comparison is difficult. Despite the discrepancies between the results of Henry's constant from this study and the known data, all the measured values are acceptable and within a reasonable range.

Table 5-4: Published data using the PPD technique to measure diffusion parameters for gas diffusion in bulk oil

Source	System	Diffusion Coefficient (m^2/s)	Henry's Constant (dimensionless)
(Zhang et al., 2000)	CH_4 – Heavy Oil	8.6×10^{-9}	-

(Li & Dong, 2009)	CH_4 – Light Oil	$(1-5.53)\times10^{-9}$	-
(Zhang et al., 2015)	CH_4 – Oil	$(0.73-5.58)\times10^{-9}$	-
(Schmdt,1989)	CH_4– Bitumen	$(0.28-1.75)\times10^{-9}$	-
(Jamialahmadi et al., 2006)	CH_4 – Heavy Oil	9.8×10^{-9}	-
(Ratnakar & Dindoruk, 2015)	CH_4 – Oil	1.23×10^{-9}	0.351
(Etminan, 2012)	CH_4 – Bitumen	0.052×10^{-9}	0.5

5.3 Estimated Diffusion Parameters in Oil-Saturated Porous Rocks

Accurately estimating diffusion coefficient of gas in bulk liquid phase has been studied by many authors as mentioned before. However, measuring the effective diffusion coefficient of the gas in the liquid-saturated porous media has been a difficult work. For now, all common analytical models are proposed to estimate diffusion coefficients of gas diffusion in bulk fluid for 1D cartesian. For radial diffusion process, there is no appropriate general analytical solution that can find diffusion parameters during the process of pressure-decay experiment. Therefore, after obtaining the pressure-decay data, the numerical model is a more practical approach to explore the result of the methane diffusion in the oil-saturated porous media corresponding this experimental methodology.

Figure 5-13 – Figure 5-15 show the density history matching of data acquired from measurements on the limestone core and Bakken shale. Henry's constant is dominant in the stabilized density or equilibrium gas pressure. All experiments for porous media are stabilized, thus, Henry's constant is fixed, and the effective diffusion coefficient will be adjusted. For limestone at the 1000 psi stage, the effective diffusion coefficient is $1.5\times10^{-10}\mathrm{m}^2/\mathrm{s}$, and the Henry's constant is 0.15. For limestone at the 2000 psi stage, the effective diffusion coefficient is

$6.5 \times 10^{-10} \mathrm{m}^2/\mathrm{s}$. The Henry's constant is 0.12. As for Bakken shale, the effective diffusion coefficient is $2 \times 10^{-11} \mathrm{m}^2/\mathrm{s}$ and the Henry's constant is 0.23.

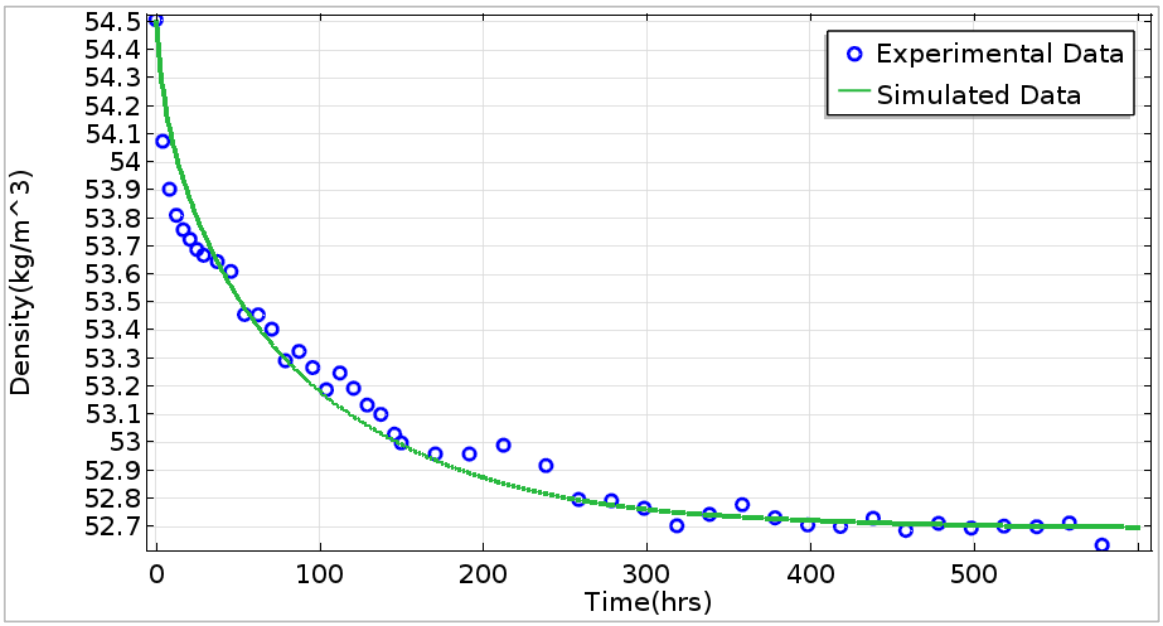

Figure 5-13: History matching of numerical model - methane diffusion in oil-saturated limestone (Low Pressure)

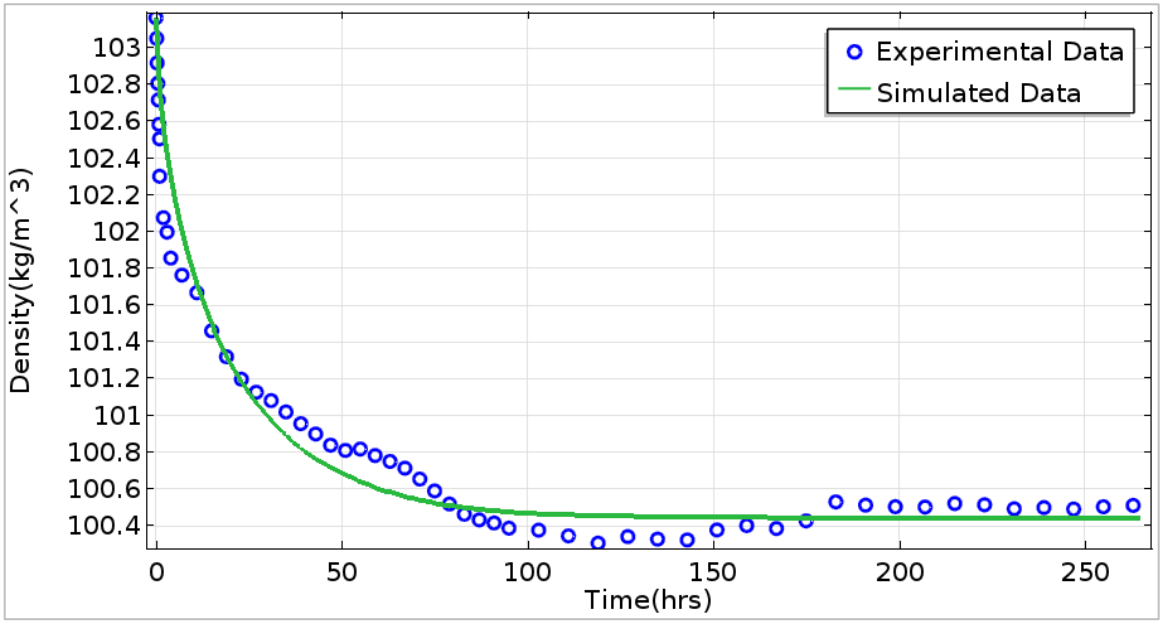

Figure 5-14: History matching of numerical model - methane diffusion in oil-saturated limestone (High Pressure)

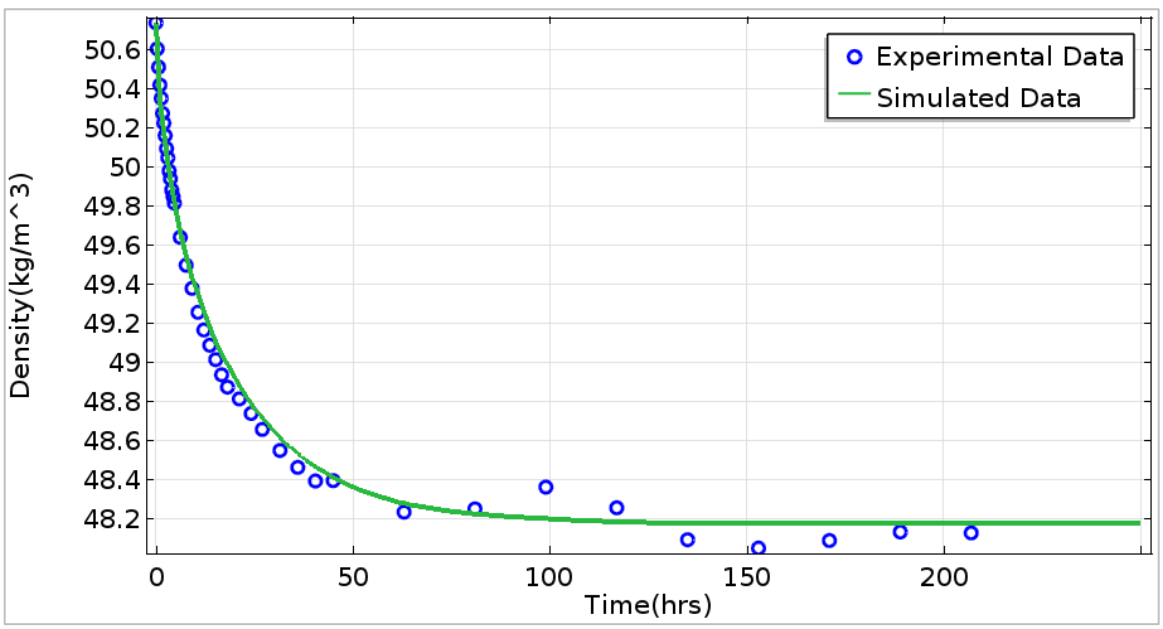

Figure 5-15: History matching of numerical model - methane diffusion in oil-saturated Bakken shale

The all measured diffusion parameters are listed in Table 5-5.

Table 5-5: Diffusion parameters obtained from numerical model

Conditions	Diffusion Coefficient (m^2/s)	Henry's Constant (dimensionless)
Methane Diffusion in Bulk Oil	3.8×10^{-9}	0.11
Methane Diffusion in Oil-Saturated Limestone (Low Pressure)	1.5×10^{-10}	0.15
Methane Diffusion in Oil-Saturated Limestone (High Pressure)	6.5×10^{-10}	0.12
Methane Diffusion in Oil-Saturated Bakken Shale	2×10^{-11}	0.23

In a porous medium, the effective diffusion coefficient decreases compared with the diffusion coefficient of the gas in bulk liquid. The diffusing molecules must move longer distance in the porous media than the bulk liquid phase. In simple terms, the complex path of connecting pores in porous media hinder the diffusion process. Tortuosity is a property of rocks, which can characterize the pore geometry of porous medium. It is an appropriate property to describe the convoluted pathways in porous rocks, which is a retardation factor that measures the resistance of a porous medium to the flow. In the fluid mechanics of porous media, tortuosity can be defined as the ratio of the effective path length (l_e) in the pore to the shortest distance (l) in a porous medium:

$$\tau = \left(\frac{l_e}{l}\right) > 1 \tag{5-1}$$

Also, in narrow liquid-filled pores, the order of magnitude of effective diffusion coefficient may be reduced through an increase in drag which in turn is due to a greater viscosity of the solvent (Grathwohl, 2012). This increase in viscosity, compared to the bulk viscosity of the solvent, is caused by the proximity of the pore wall (Cussler, 1984). This is especially applicable to small pores and narrow pore throats which have diameters in the same order of magnitude as the diffusing molecules. Thus, constrictivity is another appropriate property of a rock to explain this hindrance

effect. The dimensionless constrictivity factor (δ) relies on the ratio of the diffusing molecule diameter to the pore diameter (λ_p), which is shown in equation (5-2):

$$\lambda_p = \frac{molecule\ diameter}{pore\ diameter} < 1 \tag{5-2}$$

The following empirical equations developed by Renkin (1954) is chosen to quantify the constrictivity, because it considered hydrodynamic drag on the solute molecules due to the proximity of the pore walls in the left second term.

$$\delta = (\lambda_p)^2 (1 - 2.104\lambda_p + 2.09{\lambda_p}^3 - 0.95{\lambda_p}^5) \tag{5-3}$$

Figure 5-16 shows the other correlations between constrictivity and λ_p.

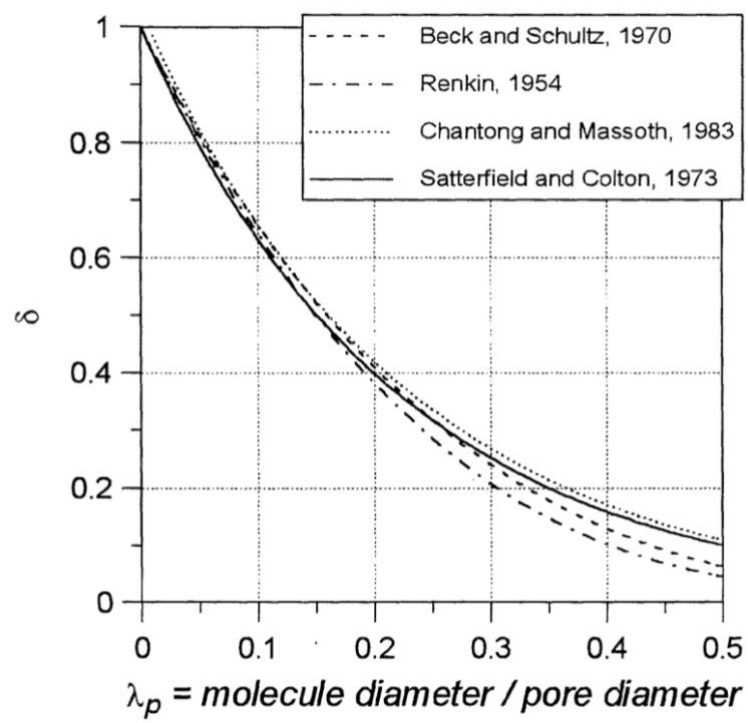

Figure 5-16: Relation between constrictivity factor and relative pore size (Grathwohl, 2012)

According to the literature, Indiana limestone are dominant by macropores (>63 μm) (Freire-Gormaly, 2013) and Bakken shale are dominant by mesopores (2-32nm) (Zhang, Sun & Ruppel, 2013). Also, the diameter of the methane molecule is nearly equal to 0.414nm. Thus, the constrictivity of the limestone and Bakken shale can be roughly estimated in this study. With the increase of the pore diameter, the constrictivity is approaching to 1 which can be negligible. On the contrary, with the decrease of the pore diameter, the constrictivity is less, leading to the stronger restricted diffusion effect.

Based on the molecular diffusion theory, Grathwohl (2012) illustrated the relation between the diffusion coefficient and effective diffusion coefficient, which can be defined as following equation:

$$D_e = \frac{D\varepsilon\delta}{\tau} \tag{5-4}$$

where D_e is the effective diffusion coefficient in porous media, D is the diffusion coefficient in bulk phase and ε is the effective transport-through porosity which accounts for the reduced cross-sectional area available for diffusion when diffusion occurs only in the pore space (no solids diffusion). In this study, effective transport-through porosity is simplified as effective porosity.

Based on the equation (5-4), tortuosity can be estimated and Table 5-6 lists the results of tortuosity.

Table 5-6: Results of estimated tortuosity

Rock	**Diffusion Coefficient (m^2/s)**	**Effective Diffusion Coefficient (m^2/s)**	**Porosity (%)**	**Constrictivity**	**Tortuosity**
Limestone	3.8×10^{-9}	1.5×10^{-10}	15-18	~1	$3.80 - 4.56$
Bakken shale	3.8×10^{-9}	2.0×10^{-11}	8	0.56-0.97	$8.51 - 14.70$

Figure 5-17 shows a comparison of the diffusion coefficients under the different tested conditions. The values are in a logarithmic scale to emphasize the order of magnitude of the diffusion coefficient. Each box represents the range of diffusion coefficients for corresponding condition, and the maximum value is on the top, while the minimum value is underneath. Therefore, we can intuitively compare the order of magnitude of diffusion coefficient for each case.

By comparing the bulk oil and porous media cases, it has been found that the limestone results are approximately one order of magnitude lower, which is a result of the restricted diffusion caused by the constrictivity and the tortuosity of the porous medium environment. The Bakken results were lower than the bulk oil results by two orders of magnitude, indicating further restricted diffusion. Bakken shale has more complex pore structure and smaller size of pores than limestone. When the diffusing molecule diameters are same, the effective diffusion coefficient decreases with the pore diameter. Also, effective diffusion coefficient decreases with the increase of the tortuosity. Due to the chosen fluids pairing, the types of porous rocks, and the experimental conditions, in this study, the sensitivity of the diffusion coefficients indicates the one order of magnitude lower.

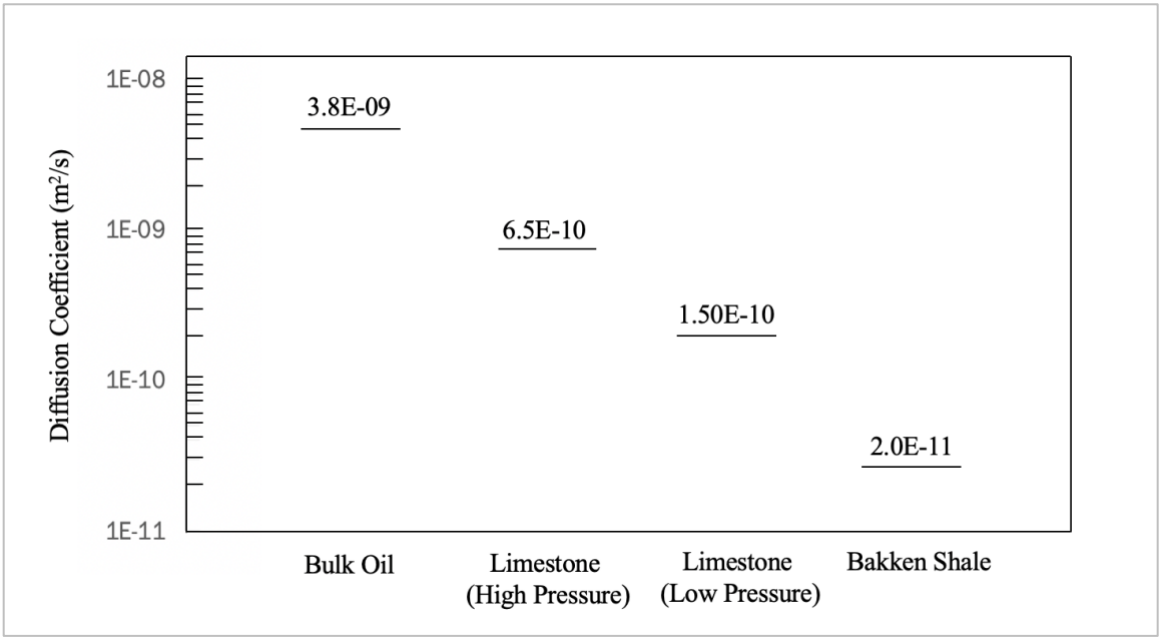

Figure 5-17: Comparison of diffusion coefficients under different conditions

Based on known tortuosity and constrictivity, a correlation between the diffusion coefficient and the effective diffusion coefficient for limestone and Bakken shale can be established. Fluids pairing is also an important factor that can affect the diffusion process, because different size of diffusing molecules can hinder the diffusion process differently, indicated by the different effective diffusion coefficients. In the simulation work, when fluids pairing changes, through the diffusion coefficient, the effective diffusion coefficient can be estimated based on this correlation. In particular, when the effective diffusion coefficients are scarce.

Basically, in convection flow, tortuosity is a function of permeability and porosity. For the flow mechanism dominated by diffusion, effective diffusion coefficient is not a function of permeability (Equation 5-4), indicating permeability and effective diffusion coefficient cannot be directly correlated. However, determining tortuosity and constrictivity have been very difficult. In contrast, permeability is easier to be measured and it can be also related to the shapes of the pores in the medium and their level of connectedness. Many researchers believe that permeability also

affects the diffusion process. Therefore, permeability can be used as an approximate indication for effective diffusion coefficients, and a simpler correlation can be found.

As suggested by Kuva et al. (2015), the matrix permeability and matrix porosity were significant physical properties for fluids diffusion in bedrock. Maarane et al. (2001) tested porosity, permeability, and diffusion coefficients by helium gas method on the diorite and granite rock samples. Boving and Grathwohl (2001) pointed out that the effective diffusion coefficient increases with the porosity, and this close relation is similar to Archie's law. Kuva et al. (2015) stated that the relation between porosity and effective diffusion coefficients revealed a weakly correlation between collected data. Also, permeability as a function of effective diffusion coefficient displayed quite strong correlation among collected data. However, these studies focus on extremely low-permeability rocks such as granite, chalk and gneiss. In this study, more tested rocks are gathered from the literature (Alharthy et al., 2017; Chen, Katz, & Tek, 1977; Hartikainen, 1998; Li & Dong, 2009, 2010; Maarane et al., 2001; Peng, Hu, & Hamamoto, 2012; Reimus, Callahan, Ware, Haga, & Counce, 2007). Due to more tested rocks, a broader range of rock properties can be explored. The diffusion coefficient here is represented as the relative diffusion coefficient, which is the ratio of the effective diffusion coefficient to the diffusion coefficients. Collected data include the gas-gas effective diffusion coefficients and the gas-liquid effective diffusion coefficients, resulting in the orders of magnitude of the two are quite different. In order to make all values comparable, all gathered values are in the logarithmic scale.

In the Figure 5-18 relation between the porosity and the relative diffusion coefficients. Based on narrow range from previous reference, there is a weakly positive correlation between the porosity and the relative diffusion coefficient for each series. However, for longer range of the porosity, it is difficult to confirm that the relative diffusion coefficient increases with the porosity or that there is a positive correlation between the two. The possible reason is that gathered data are

still scare relatively. More data are missing in the big map, forcing the relation looks like a positive correlation.

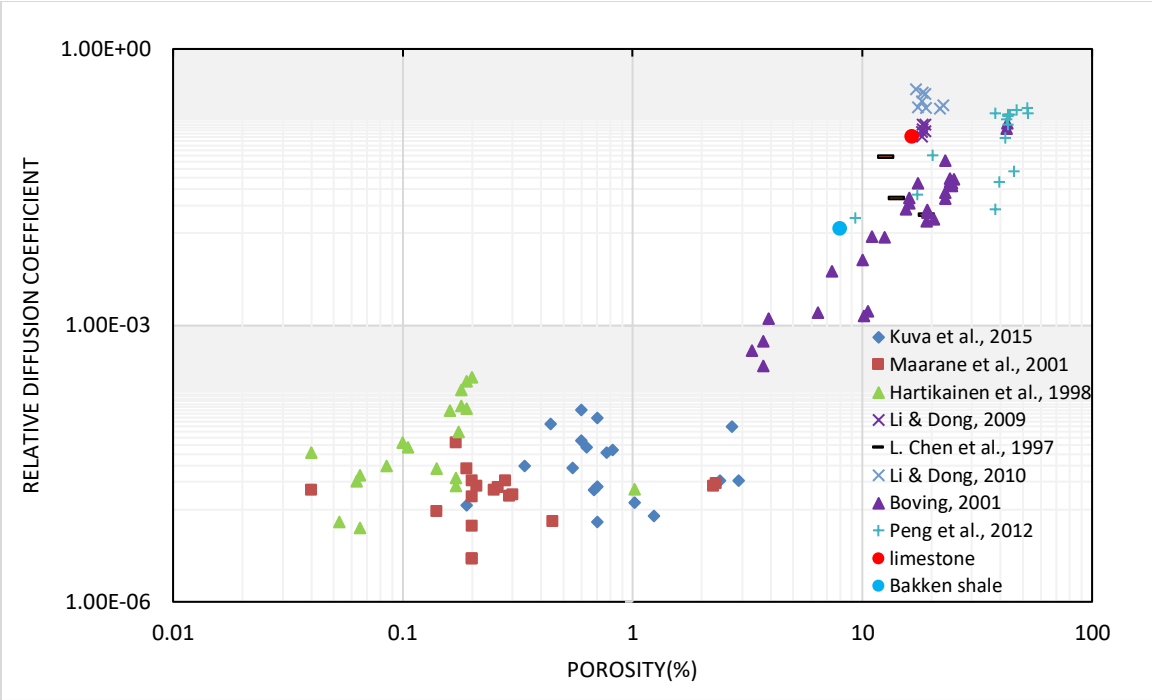

Figure 5-18 Relation between relative diffusion coefficient and porosity

In Figure 5-19, the relation between the permeability and the relative diffusion coefficient is exhibited. Through the observation, the weak positive correlation between permeability and diffusion coefficient is more obvious. In general, the relative diffusion coefficient increases with permeability. On the average, data points roughly obey a power-law function: $y = 3E+06x^{0.5988}$, and R square is 0.822, indicating that the correlation between the permeability and the relative diffusion coefficient is high.

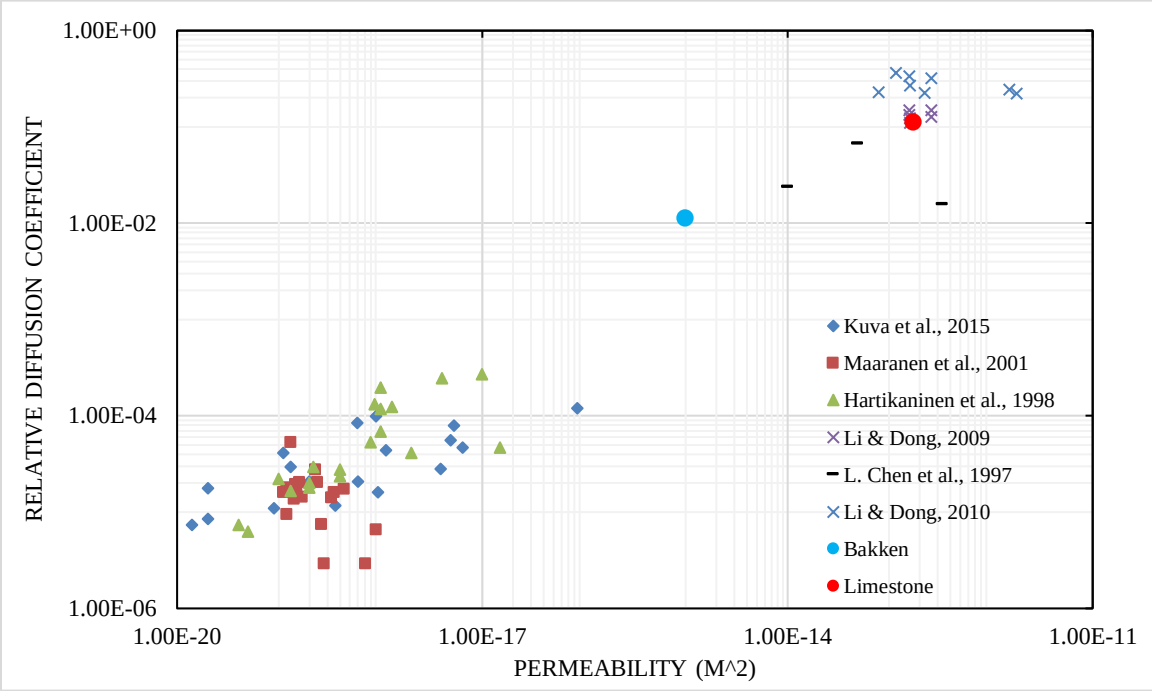

Figure 5-19: Relation between relative diffusion coefficient and permeability

Then, in order to determine whether both porosity and permeability can yield a significantly better predictive capability of relative diffusion coefficient than either variable alone, multiple linear regression was used to explain the relation between one continuous dependent variable (relative diffusion coefficient) and two independent variables (permeability and porosity). The resulting multiple linear regression equation is as follows:

$$\log\left(\frac{D_e}{D}\right) = 5.15525 + 0.51234\log(\mathrm{k}) + 0.46573\log(\phi) \tag{5-1}$$

Where D_e is effective diffusion coefficient, D is the diffusion coefficient, k is the matrix permeability, and ϕ is porosity.

Table 5-7 shows relevant regression parameters obtained. R square is equal to 0.85, which is a little bit larger than 0.82, demonstrating porosity has only a slight effect on the diffusion coefficient. Although the p-values for permeability and porosity are smaller than the significance

level of 0.05, the relative diffusion coefficient is more highly-correlated with matrix permeability and matrix porosity by comparing their p-values. Hence, for the prediction of the effective diffusion coefficient, the permeability has a greater influence on the effective diffusion coefficient than does porosity, because fluids diffusion in the rock matrix must occur through the well-connected pores. If the pores are not connected, fluids cannot flow in the matrix no matter how high the porosity. Therefore, diffusion depends on permeability rather than on pore volumes.

Table 5-7: Relevant parameters obtained from linear multiple regression

Methods	Coefficient	P-value	R Square
Intercept	5.155258849	1.62732E-07	
log(permeability)	0.512344321	1.23267E-14	0.848493999
log(porosity)	0.465730539	0.001320687	

Chapter 6

Conclusions

In this work, a practical modified pressure-decay experimental methodology has been developed and tested to obtain more reliable gas-liquid diffusion data in oil-saturated porous rocks, especially for tight rocks. Three different modeling approaches are implemented for estimating diffusion coefficients and the diffusion parameters obtained from these modeling methods are in agreement with data published in the literature. Therefore, a more complete library of effective diffusion coefficients can be created based on this procure.

The following conclusions can be drawn from the results of our study,

1. The phenomenon of hindered diffusion in porous media was clearly observed in our experiments. The diffusion coefficient of methane in bulk Bakken oil was estimated at $3.8 \times 10^{-9}\ \mathrm{m}^2/\mathrm{s}$ whereas the effective diffusion coefficients of methane in oil-saturated high porosity-permeability limestone was between $1.5\times 10^{-10}\ \mathrm{m}^2/\mathrm{s}$ and $6.5 \times 10^{-10}\ \mathrm{m}^2/\mathrm{s}$, an order of magnitude reduction. This hindrance to diffusion was even more significant in low porosity-permeability Bakken shale samples with effective diffusion coefficients estimated at $2.0 \times 10^{-11}\ \mathrm{m}^2/\mathrm{s}$, a further order of magnitude reduction.

2. Effective diffusion coefficient was found to decrease with the decrease of constrictivity factor, and decreases with the increase of tortuosity. The lower constrictivity factor and greater tortuosity can lead to the stronger restricted diffusion as a result of smaller pore size and more tortuous pore network.

3. This work successfully correlates the diffusion coefficient of bulk fluids (gas to oil) against the effective diffusion coefficient in porous rocks employing the lab measurements and numerical simulation results: By employing the molecular diffusion theory, one can acquire the

constrictivity factor and tortuosity for particular rocks, thus obtaining effective diffusion coefficients for various fluid pairings in the same rock.

Diffusion is an important transport phenomenon in tight reservoirs and this work lays a foundation to obtain effective diffusion coefficients for various fluid pairings in both conventional and tight rocks. This critical input data for reservoir and production simulation is rarely available and often approximated from inappropriate analogs such as bulk fluid diffusion.

Chapter 7

Recommendations for Future Work

The results of this study provide a procedure for correlating the diffusion coefficient to the effective diffusion coefficient in limestone and Bakken shale. This encourages more independent experimental data to support or improve the correlation between the diffusion coefficient and the effective diffusion coefficient. However, molecular diffusion theory is not the best understood technique to estimate the tortuosity. The results of the tortuosity and pore size distributions need to be more carefully validated so that correlations can be established more correct. The results also indicate that Bakken shale is not like traditional shale such as Marcellus shale with extremely low-injectivity. More porous media with more complex geometric pore structure, micropores/nanopores or different composition should be deeper investigated to validate the feasibility of this experimental methodology. Furthermore, experiments under various conditions of combinations of fluids, as well as at higher pressure-temperature conditions would also be useful to improve the experimental setup for more universal applications.

The effect of oil-swelling is often negligible in the fluids transport models because the oil compressibility can be neglected for the most of heavy oils. However, when the liquid is light oil, the oil volume is relatively small or the gas-liquid interface area is small, the swelling effect may not be neglected. Furthermore, the composition of the oil is changing during the diffusion process, indicating that the diffusion coefficient is always changing with time. Also, although there is no overall convection in the closed system, the potential effect of convection for porous media should be validated in the model. Such negligible factors should be considered in the assumption to constrain the model and help better describe the corresponding experiment.

References

Alharthy, N., Teklu, T. W., Kazemi, H., Graves, R. M., Hawthorne, S. B., Braunberger, J., & Kurtoglu, B. (2018). Enhanced Oil Recovery in Liquid-Rich Shale Reservoirs: Laboratory to Field. *SPE Reservoir Evaluation & Engineering*, *21*(01), 137–159. https://doi.org/10.2118/175034-PA

Amann-Hildenbrand, A., Ghanizadeh, A., & Krooss, B. M. (2012). Transport properties of unconventional gas systems. *Marine and Petroleum Geology*, *31*(1), 90–99. https://doi.org/10.1016/j.marpetgeo.2011.11.009

Bardon, L., & Denoyelle, L. (2012). *Heavy Crude Oil Recovery*. *Heavy Crude Oil Recovery*. https://doi.org/10.1007/978-94-009-6140-1

Boving, T., & Grathwohl, P. (2001). Tracer Diffusion Coefficients in Sedimentary rocks: Correlation to Porosity and Hydraulic Conductivity. *Journal of Contaminant Hydrology*.

Brenner, H., & Leal, L. G. (1978). Interfacial resistance to interphase mass transfer in quiescent two-phase systems. *AIChE Journal*, *24*(2), 246–254. https://doi.org/10.1002/aic.690240213

Carlson, E. S., & Mercer, J. C. (1991). Devonian shale gas production: mechanisms and simple models. Journal of Petroleum technology, 43(04), 476-482.

Chen, L. L., Katz, D. L., & Tek, M. R. (1977). Binary gas diffusion of methane-nitrogen through porous solids. AIChE Journal, 23(3), 336–341. https://doi.org/10.1002/aic.690230317

Civan, F., & Maurice, R. (2001). Accurate Measurement of Gas Diffusivity in Oil and Brine Under Reservoir Conditions, 1–11. https://doi.org/10.2523/67319-MS

Civan, F., & Rasmussen, M. L. (2002). Improved measurement of gas diffusivity for miscible gas flooding under nonequilibrium vs. equilibrium conditions. In SPE/DOE Improved Oil Recovery Symposium. Society of Petroleum Engineers.

Creux, P., Meyer, V., Cordelier, P. R., Franco, F., & Montel, F. (2005). Diffusivity in heavy oils. In SPE International Thermal Operations and Heavy Oil Symposium. Society of Petroleum Engineers.

Cussler, E. L., Stokar, M. R., & Varberg, J. E. (1984). Gels as size selective extraction solvents. AIChE journal, 30(4), 578-582.

Energy Information Administration. 2014. Outlook for U.S. Shale Oil and Gas, https://www.eia.gov/pressroom/presentations/sieminski_01042014.pdf

Energy Information Administration. 2019. Bakken Region - Drilling Productivity Report. https://www.eia.gov/petroleum/drilling/pdf/bakken.pdf

Ertekin, T., King, G. A., & Schwerer, F. C. (2007). Dynamic Gas Slippage: A Unique Dual-Mechanism Approach to the Flow of Gas in Tight Formations. SPE Formation Evaluation, 1(01), 43–52. https://doi.org/10.2118/12045-PA

Etminan, S. R. (2012). Determination of Mass Transfer Parameters in Solvent-Based Oil Recovery Processes. In SPE Annual Technical Conference and Exhibition. Society of Petroleum Engineers.

Etminan, S. R., Maini, B. B., Chen, Z., & Hassanzadeh, H. (2010). Constant-pressure technique for gas diffusivity and solubility measurements in heavy oil and bitumen. Energy and Fuels, 24(1), 533–549. https://doi.org/10.1021/ef9008955.

Etminan, S. R., Maini, B. B., Hassanzadeh, H., & Chen, Z. J. (2009). Determination of Concentration Dependent Diffusivity Coefficient in Solvent Gas Heavy Oil Systems. https://doi.org/10.2118/124832-MS

Freeman, C., Moridis, G., & Blasingame, T. (2011). A Numerical Study of Microscale Flow Behavior in Tight Gas and Shale Gas Reservoir Systems. *Transport in Porous Media*, *90*(1), 253–268. https://doi.org/10.1007/s11242-011-9761-6

Freire-Gormaly, M. (2013). The pore structure of Indiana limestone and pink dolomite for the modeling of carbon dioxide in geologic carbonate rock formations. University of Toronto.

French, S., Rodgerson, J., & Feik, C. (2014). Re-fracturing Horizontal Shale Wells: Case History of a Woodford Shale Pilot Project, 1–24. https://doi.org/10.2118/168607-MS

Gamadi, T. D., Sheng, J. J., Soliman, M. Y., Menouar, H., Watson, M. C., & Emadibaladehi, H. (2014). An Experimental Study of Cyclic CO2 Injection to Improve Shale Oil Recovery, 1–9. https://doi.org/10.2118/169142-MS

Ghaderi, S. M., Tabatabaie, S. H., Hassanzadeh, H., & Pooladi-Darvish, M. (2011). Estimation of concentration-dependent diffusion coefficient in pressure-decay experiment of heavy oils and bitumen. *Fluid Phase Equilibria*, *305*(2), 132–144. https://doi.org/10.1016/j.fluid.2011.03.010

Grabanski, C. B., Sorensen, J. A., Burton-Kelly, M. E., Smith, S. A., Miller, D. J., Bosshart, N. W., Jin, L. (2016). Improving Oil Transportability Using CO2 in the Bakken System – A Laboratory Investigation. https://doi.org/10.2118/178948-MS

Grathwohl, P. (2012). Diffusion in natural porous media: contaminant transport, sorption/desorption and dissolution kinetics (Vol. 1). Springer Science & Business Media.

Han, F., Busch, A., Krooss, B. M., Liu, Z., Van Wageningen, N., & Yang, J. (2010). Experimental study on fluid transport processes in the cleat and matrix systems of coal. *Energy and Fuels*, *24*(12), 6653–6661. https://doi.org/10.1021/ef100165w

Hartikainen, K., & Hartikainen, J. (1998). Posivas site investigations in Olkiluoto, Kivetty, Romuvaara and Hästholmen by He-gas methods in 1997. Posiva Working Report.

Henry, W. (1803). Experiments on the Quantity of Gases Absorbed by Water , at Different Temperatures , and under Different Pressures. *Philosophical Transactions of the Royal Society of London*, *93*(29), 274.

Hoffman, B. T. (2012). Comparison of Various Gases for Enhanced Recovery from Shale Oil Reservoirs, (1), 1–8. https://doi.org/10.2118/154329-MS

Hoteit, H., & Firoozabadi, A. (2006, January). Numerical modeling of diffusion in fractured media for gas injection and recycling schemes. In SPE Annual Technical Conference and Exhibition. Society of Petroleum Engineers.

Imai, M., Sumikawa, I., Yamada, T., & Nakano, M. (2012). Reservoir Fluid Characterization for Tight Fractured Reservoirs: Effect of Diffusion, (1982). https://doi.org/10.2118/158884-MS

Jacobs, T. (2014). Renewing mature shale wells through refracturing. Journal of Petroleum Technology, 66(04), 52-60.

Jamialahmadi, M., Emadi, M., & Müller-Steinhagen, H. (2006). Diffusion coefficients of methane in liquid hydrocarbons at high pressure and temperature. *Journal of Petroleum Science and Engineering*, *53*(1–2), 47–60. https://doi.org/10.1016/j.petrol.2006.01.011

Johns, R. T., & Dindoruk, B. (2013). Enhanced Oil Recovery Field Case Studies: Chapter 1. Gas Flooding. Elsevier Inc. Chapters.

Kojadinovich, G. (2018). Laboratory Investigation of Oil-Composition Affecting the Success of Low-Salinity Waterflooding in Oil-Wet Carbonate Rocks (Master Thesis, Pennsylvania State University).

Kovaleva, L., Davletbaev, A., Babadagli, T., & Stepanova, Z. (2011). Effects of electrical and radio-frequency electromagnetic heating on the mass-transfer process during miscible injection for heavy-oil recovery. *Energy and Fuels*, *25*(2), 482–486. https://doi.org/10.1021/ef1009428

Kuva, J., Voutilainen, M., Kekäläinen, P., Siitari-Kauppi, M., Timonen, J., & Koskinen, L. (2015). Gas Phase Measurements of Porosity, Diffusion Coefficient, and Permeability in Rock Samples from Olkiluoto Bedrock, Finland. *Transport in Porous Media*, *107*(1), 187–204. https://doi.org/10.1007/s11242-014-0432-2

Li, H., & Yang, D. (2015). Determination of Individual Diffusion Coefficients of Solvent/CO_2 Mixture in Heavy Oil With Pressure-Decay Method. *SPE Journal*, *21*(01), 131–143. https://doi.org/10.2118/176032-PA

Li, Z., & Dong, M. (2009). Experimental Study of Carbon Dioxide Diffusion in Oil-Saturated Porous Media. *Industrial and Engineering Chemistry Research*, *48*(20), 9307–9317. https://doi.org/10.1021/ie900145c

Li, Z., & Dong, M. (2010). Experimental study of diffusive tortuosity of liquid-saturated consolidated porous media. *Industrial and Engineering Chemistry Research*, *49*(13), 6231–6237. https://doi.org/10.1021/ie901765d

Liu, Y., Teng, Y., Lu, G., Jiang, L., Zhao, J., Zhang, Y., & Song, Y. (2016). Experimental study on CO2 diffusion in bulk n-decane and n-decane saturated porous media using micro-CT. *Fluid Phase Equilibria*, *417*, 212–219. https://doi.org/10.1016/j.fluid.2016.02.034

Luo, H., Kryuchkov, S., & Kantzas, A. (2007). The Effect of Volume Changes Due to Mixing on Diffusion Coefficient Determination in Heavy Oil and Hydrocarbon Solvent System, *C*(2). https://doi.org/10.2118/110522-MS

Maaranen, J., Lehtioksa, J., & Timonen, J. (2001). Determination of porosity, permeability and diffusivity of rock samples from Äspö hrl using the helium gas method. Äspö Hard Rock Laboratory International Progress Report IPR-02-17, Svensk Kärnbränslehantering AB.

Marlowe, M. O., & Kaznoff, A. I. (1968). Tracer study of the surface diffusivity of UO2. Jo*urnal of Nuclear Materials*, *25*(3), 328–333. https://doi.org/10.1016/0022-3115(68)90178-5

Mikkelsen, J. C. (1982). Diffusivity of oxygen in silicon during steam oxidation. *Applied Physics Letters*, *40*(4), 336–337. https://doi.org/10.1063/1.93089

Nakashima, Y. (2000). The use of X-ray CT to measure diffusion coefficients of heavy ions in water-saturated porous media. *Developments in Geotechnical Engineering*, *84*(C), 11–17. https://doi.org/10.1016/S0165-1250(00)80003-6

Nour, A. H., Yaacob, Z. Bin, & Alagorni, A. H. (2015). An Overview of Oil Production Stages: Enhanced Oil Recovery Techniques and Nitrogen Injection. *International Journal of Environmental Science and Development*, *6*(9), 693–701. https://doi.org/10.7763/ijesd.2015.v6.682

Pacheco, F., & Hejazi, H. (2015). Estimation of Solubility and Diffusivity of Gases in Heavy Oils by Use of Late-Time Pressure-Decay Data: An Analytical/Graphical Approach. *SPE Journal*, *20*(04), 717–728. https://doi.org/10.2118/170957-PA

Peng, S., Hu, Q., & Hamamoto, S. (2012). Diffusivity of rocks: Gas diffusion measurements and correlation to porosity and pore size distribution. *Water Resources Research*, *48*(2), 1–9. https://doi.org/10.1029/2011WR011098

Pomeroy, R. D., Lacey, W. N., Scudder, N. F., & Stapp, F. P. (1933). Rate of Solution of Methane in Quiescent Liquid Hydrocarbons. *Industrial and Engineering Chemistry*, *25*(9), 1014–1019. https://doi.org/10.1021/ie50285a021

Rahmanian, M., Aguilera, R., & Kantzas, A. (2013). A New Unified Diffusion--Viscous-Flow Model Based on Pore-Level Studies of Tight Gas Formations. *SPE Journal*, *18*(01), 38–49. https://doi.org/10.2118/149223-PA

Rao, D. (2001). Gas injection EOR - a new meaning in the new millennium. *Journal of Canadian Petroleum Technology*, *40*(2), 11–19. https://doi.org/10.2118/01-02-DAS

Ratnakar, R., & Dindoruk, B. (2015a). Measurement of Gas Diffusivity in Heavy Oils and Bitumens by Use of Pressure-Decay Test and Establishment of Minimum Time Criteria for Experiments. *SPE Journal*, *20*(05), 1167–1180. https://doi.org/10.2118/170931-PA

Ratnakar, R., & Dindoruk, B. (2015b). Measurement of Gas Diffusivity in Heavy Oils and Bitumens by Use of Pressure-Decay Test and Establishment of Minimum Time Criteria for Experiments. *SPE Journal*, *20*(05), 1167–1180. https://doi.org/10.2118/170931-PA

Ratnakar, R., & Dindoruk, B. (2016). On the Exact Representation of Pressure Decay Tests: New Modeling and Experimental Data for Diffusivity Measurement in Gas - Oil/Bitumen Systems. https://doi.org/10.2118/181514-MS

Ratnakar, R., & Dindoruk, B. (2018). Effect of GOR on Gas Diffusivity in Reservoir Fluid Systems, (September), 24–26. https://doi.org/10.2118/191531-MS

Reimus, P. W., Callahan, T. J., Ware, S. D., Haga, M. J., & Counce, D. A. (2007). Matrix diffusion coefficients in volcanic rocks at the Nevada test site: Influence of matrix porosity, matrix

permeability, and fracture coating minerals. *Journal of Contaminant Hydrology*, *93*(1–4), 85–95. https://doi.org/10.1016/j.jconhyd.2007.01.017

Renner, T. A. (1988). Measurement and Correlation of Diffusion Coefficients for CO2 and Rich-Gas Applications. *SPE Reservoir Engineering*, *3*(02), 517–523. https://doi.org/10.2118/15391-PA

Riazi, M. R. (1996). A new method for experimental measurement of diffusion coefficients in reservoir fluids. *Journal of Petroleum Science and Engineering*, *14*(3–4), 235–250. https://doi.org/10.1016/0920-4105(95)00035-6

Schmidt, T. "Mass transfer by diffusion" AOSTRA Technical Handbook on Oil Sands,Bitumens and Heavy Oils. Alberta Oil Sand Technology and Research Authority,Edmonton, Canada, pp. 311-332. 1989.

Sheikha, H., Pooladi-Darvish, M., & Mehrotra, A. K. (2005). Development of graphical methods for estimating the diffusivity coefficient of gases in bitumen from pressure-decay data. *Energy and Fuels*, *19*(5), 2041–2049. https://doi.org/10.1021/ef050057c

Sheng, J. J. (2015). Enhanced oil recovery in shale reservoirs by gas injection. *Journal of Natural Gas Science and Engineering*, *22*, 252–259. https://doi.org/10.1016/j.jngse.2014.12.002

Simpliciano, C., Clark, L., Asi, B., Chu, N., Mercado, M., Diaz, S., Miremadi, M. (2013). Cross-Linked Alginate Film Pore Size Determination Using Atomic Force Microscopy and Validation Using Diffusivity Determinations. *Journal of Surface Engineered Materials and Advanced Technology*, *03*(04), 1–12. https://doi.org/10.4236/jsemat.2013.34a1001

Taylor, D., & Bushell, M. (1985). The spatial mapping of translational diffusion coefficients by the NMR imaging technique. *Physics in Medicine and Biology*, *30*, 345–349. https://doi.org/10.1088/0031-9155/30/4/009

Teletzke, G. F., Patel, P. D., & Chen, A. (2005). Methodology for Miscible Gas Injection EOR Screening. In *SPE International Improved Oil Recovery Conference in Asia Pacific*. https://doi.org/10.2118/97650-MS

Tharanivasan, A. K., Yang, C., & Gu, Y. (2004). Comparison of three different interface mass transfer models used in the experimental measurement of solvent diffusivity in heavy oil. *Journal of Petroleum Science and Engineering*, *44*(3–4), 269–282. https://doi.org/10.1016/j.petrol.2004.03.003

Tharanivasan, A. K., Yang, C., & Gu, Y. (2006). Measurements of molecular diffusion coefficients of carbon dioxide, methane, and propane in heavy oil under reservoir conditions. *Energy and Fuels*, *20*(6), 2509–2517. https://doi.org/10.1021/ef060080d

Thomas, G., & Monger, T. (2007). Feasibility of Cyclic CO2 Injection for Light-Oil Recovery. *SPE Reservoir Engineering*, *6*(02), 179–184. https://doi.org/10.2118/20208-PA

Thomas, S. (2008). Enhanced Oil Recovery - An Overview. *Oil & Gas Science and Technology*, *63*(2–3), 474–486. https://doi.org/10.2516/ogst

Upreti, S. R., & Mehrotra, A. K. (2002). Diffusivity of CO2, CH4, C2H6 and N2 in Athabasca bitumen. *Canadian Journal of Chemical Engineering*, *80*(1), 116–125. https://doi.org/10.1002/cjce.5450800112

Wan, T., Sheng, J., Soliman, M., & Zhang, Y. (2016). Effect of Fracture Characteristics on Behavior of Fractured Shale-Oil Reservoirs by Cyclic Gas Injection. *SPE Reservoir Evaluation & Engineering*, *19*(02), 350–355. https://doi.org/10.2118/168880-PA

Wang, C., & Li, S. (2019). The effect of fractures on gas injection in Hailar oilfield. *Journal of Petroleum Exploration and Production Technology*, *9*(1), 409–416. https://doi.org/10.1007/s13202-018-0475-y

Wang, C., & Li, X. (2018). The Empirical and Theoretical Miscible Characterization Method in Gas-Enhanced Oil Recovery. *Geofluids*, *2018*, 1–9. https://doi.org/10.1155/2018/7841948

Wen, Y., Kantzas, A., & Wang, G. J. (2010). Estimation of Diffusion Coefficients in Bitumen Solvent Mixtures Using X-Ray CAT Scanning and Low Field NMR, (6). https://doi.org/10.2118/2004-064

Yang, Z., Dong, M., Gong, H., & Li, Y. (2017). Determination of Mass Transfer Coefficient of Methane in Heavy Oil-Saturated Unconsolidated Porous Media Using Constant-Pressure Technique.

Industrial and Engineering Chemistry Research, *56*(25), 7390–7400. https://doi.org/10.1021/acs.iecr.7b01088

Yu, W., Lashgari, H. R., Wu, K., & Sepehrnoori, K. (2015). CO2 injection for enhanced oil recovery in Bakken tight oil reservoirs. *Fuel*, *159*, 354–363. https://doi.org/10.1016/j.fuel.2015.06.092

Yu, W., Lashgari, H., & Sepehrnoori, K. (2014). Simulation Study of CO2 Huff-n-Puff Process in Bakken Tight Oil Reservoirs, *2*(April), 16–18. https://doi.org/10.2118/169575-ms

Yuan, W., Pan, Z., Li, X., Yang, Y., Zhao, C., Connell, L. D., He, J. (2014). Experimental study and modelling of methane adsorption and diffusion in shale. *Fuel*, *117*(PART A), 509–519. https://doi.org/10.1016/j.fuel.2013.09.046

Zhang, M., Chakraborty, N., Karpyn, Z., Emami-meybodi, H., Ayala, L., & Pennsylvania, T. (2019). Numerical and Experimental Analysis of Diffusion and Sorption Kinetics Effects in Marcellus Shale Gas Transport Single-Component Gas Transport Model in Shale Nanopores.

Zhang, T., Sun, X., & Ruppel, S. (2013, March). Hydrocarbon geochemistry and pore characterization of Bakken Formation and implications to oil migration and oil saturation. In SDA from AAPG Annual Convention, Pittsburg.

Zhang, Y., Hyndman, C., & Maini, B. (2000). Measurement of gas diffusivity in heavy oils. *Journal of Petroleum Science and Engineering*, *25*(1–2), 37–47. https://doi.org/10.1016/S0920-4105(99)00031-5

Zhang, Y., Sun, X., Duan, X., & Li, X. (2015). Diffusion coefficients of natural gas in foamy oil systems under high pressures. *Petroleum Science*, *12*(2), 293–303. https://doi.org/10.1007/s12182-015-0023-z

Zuloaga, P., Yu, W., Miao, J., & Sepehrnoori, K. (2017). Performance evaluation of CO2 Huff-n-Puff and continuous CO2 injection in tight oil reservoirs. *Energy*, *134*, 181–192. https://doi.org/10.1016/j.energy.2017.06.028

Appendix A

Equations in the Simplified Graphical Approach

Relation between H_{ij} and K_H

Henry's law is used to relate gas concentration and oil/gas interface with gas partial pressure:

$$P = H_{ij} C_{Go,int} \tag{B-1}$$

Where P is gas cap pressure, H_{ij} is Henry's constant, and $C_{Go,int}$ is the equilibrium gas concentration at the interface.

K_H is another dimensionless form of Henry's constant, also refers to equilibrium concentration. The definition of K_H is shown below:

$$K_H = \frac{C_{Go,int}}{C_{Gg}} \tag{B-2}$$

Gas concentration in gas cap is 100%, thus:

$$C_{Go,int} = \rho_g = \frac{PM}{ZRT} \tag{B-3}$$

Where ρ_g is the density of gas in gas cap, M is the molar weight of gas, Z is gas-compressibility factor, R is universal gas constant, and T is temperature.

By substituting Equation (B-1) and (B-3) into Equation (B-2):

$$\frac{1}{K_H} = H_{ij} \frac{PM}{ZRT} \tag{B-4}$$

Based on previous study from Pacheco & Heijazi, (2015):

$$\frac{\psi}{h_L} = \frac{M}{ZRT} \tag{B-5}$$

By substituting Equation (B-5) into Equation (B-4), the relation between H_{ij} and K_H can be obtained:

$$K_H = \frac{h_L}{\psi H_{ij}} \tag{B-6}$$

Simplified integral procedure

The concentration profile is described by Equation (B-8) from (Ratnakar & Dindoruk, 2015b):

$$\rho_g(t) = \rho_{g\infty} + \beta \exp(-m_2 t) \tag{B-7}$$

Then, take the logarithm of both sides:

$$\rho_g(t) - \rho_{g\infty} = ln\beta - m_2 t \tag{B-8}$$

If differentiate both sides of Equation (B-9) with respect to t, the following equation can be obtained:

$$\frac{d[\rho_g(t) - \rho_{g\infty}]}{dt} = -m_2[\rho_g(t) - \rho_{g\infty}] \tag{B-9}$$

Take the quadratic derivative of both sides of Equation (B-11):

$$\frac{d^2[\rho_g(t) - \rho_{g\infty}]}{dt^2} = -m_2 \frac{d[\rho_g(t) - \rho_{g\infty}]}{dt} \tag{B-10}$$

The right-hand side of Equation (B-11) can be rewritten by substituting Equation (B-10) into Equation(B-11), the following equation displays the result:

$$\frac{d^2[\rho_g(t) - \rho_{g\infty}]}{dt^2} = -{m_2}^2[\rho_g(t) - \rho_{g\infty}] \tag{B-11}$$

Then, integrate time from *t* to t_f:

$$\int_t^{t_f} \left\{\frac{d^2[\rho_g(t) - \rho_{g\infty}]}{dt^2}\right\} \mathrm{dt} = {m_2}^2 \int_t^{t_f} \rho_g(t)dt - \rho_{g\infty}{m_2}^2(t_f - t) \tag{B-12}$$

By substituting Equation (B-12) into Equation (B-13), the final equation from the simplified graphical approach for calculate equilibrium concentration can be revealed as following equation:

$$\frac{1}{\rho(t) - \rho_{t_f}} \int_{t}^{t_f} \rho(t) dt = \rho_{g\infty} \left[\frac{t_f - t}{\rho(t) - \rho_{t_f}} \right] + \frac{1}{m_2} \tag{B-13}$$

Appendix B

Literature Data

Values of the diffusion coefficients, porosity and permeability, which are reported in Table B-1, were collected from the different references.

Table B-1: The properties of rocks obtained from the literature

Source	Rock Type	effective diffusion coefficient (m^2/s)	relative diffusion coefficient (m^2/s)	porosity (%)	permeability (m^2)
(Kuva et al., 2015)	Pegmatitic granite	8.20E-09	1.21E-04	0.6	8.60E-17
	Pegmatitic granite	3.20E-09	4.74E-05	0.63	6.40E-18
	Pegmatitic granite	5.70E-09	8.44E-05	0.44	5.90E-19
	Veined gneiss	6.70E-09	9.93E-05	0.7	9.00E-19
	Veined gneiss	2.00E-09	2.96E-05	0.34	1.30E-19
	Veined gneiss	1.40E-09	2.07E-05	2.4	6.00E-19
	Veined gneiss	2.80E-09	4.15E-05	0.77	1.10E-19
	Veined gneiss	3.80E-09	5.63E-05	0.6	4.90E-18
	Veined gneiss	1.90E-09	2.81E-05	0.55	3.90E-18
	Veined gneiss	3.00E-09	4.44E-05	0.82	1.13E-18
	Veined gneiss	5.80E-10	8.59E-06	1.24	2.00E-20

	Veined gneiss	5.40E-09	8.00E-05	2.7	5.30E-18
	Veined gneiss	5.00E-10	7.41E-06	0.7	1.40E-20
	Veined gneiss	7.50E-10	1.11E-05	0.19	9.00E-20
	Veined gneiss	8.00E-10	1.19E-05	1.02	3.60E-19
	Veined gneiss	1.40E-09	2.07E-05	2.9	2.00E-19
	Veined gneiss	1.10E-09	1.63E-05	0.68	9.50E-19
	Veined gneiss	1.20E-09	1.78E-05	0.7	2.00E-20
(Maarane et al., 2001)	diorite	1.10E-09	1.62E-05	0.25	1.10E-19
	diorite	1.23E-09	1.81E-05	2.24	1.49E-19
	diorite	1.32E-09	1.95E-05	2.3	1.45E-19
	diorite	1.39E-09	2.05E-05	0.28	1.60E-19
	diorite	1.22E-09	1.80E-05	0.21	1.20E-19
	diorite	9.60E-10	1.42E-05	0.29	3.30E-19
	diorite	1.18E-09	1.74E-05	0.26	4.40E-19
	granite	3.60E-09	5.31E-05	0.17	1.30E-19
	granite	2.00E-10	2.95E-06	0.2	2.80E-19
	granite	9.40E-10	1.39E-05	0.2	1.40E-19

	granite	1.90E-09	2.80E-05	0.19	2.30E-19
	granite	6.50E-10	9.59E-06	0.14	1.20E-19
	diorite	1.10E-09	1.62E-05	0.04	3.50E-19
	diorite	9.80E-10	1.45E-05	0.3	1.70E-19
	diorite	2.00E-10	2.95E-06	0.2	7.10E-19
	diorite	5.10E-10	7.52E-06	0.45	2.60E-19
	diorite	4.50E-10	6.64E-06	0.2	9.00E-19
	diorite	1.40E-09	2.06E-05	0.2	2.40E-19
(Hartikainen, 1998)	granite	4.70E-09	6.93E-05	0.175	1.00E-18
	granite	1.85E-08	2.73E-04	0.2	1.00E-17
	Mica gneiss	1.50E-09	2.21E-05	0.17	1.00E-19
	Mica gneiss	5.00E-10	7.37E-06	0.053	4.00E-20
	Tonalite	2.80E-09	4.13E-05	0.04	2.00E-18
	Tonalite	1.23E-09	1.81E-05	0.17	2.00E-19
	Porphyritic granodiorite	3.60E-09	5.31E-05	0.1	8.00E-19
	Porphyritic granodiorite	1.38E-09	2.04E-05	0.063	2.00E-19
	Porphyritic granite	8.05E-09	1.19E-04	0.16	1.00E-18

	gneiss	1.67E-08	2.46E-04	0.19	4.00E-18
	gneiss	1.13E-09	1.67E-05	1.02	1.30E-19
	Amfibolite	8.50E-09	1.25E-04	0.19	1.30E-18
	Amfibolite	4.30E-10	6.34E-06	0.065	5.00E-20
	Amfibolite	1.88E-09	2.77E-05	0.14	4.00E-19
	Granodiorite	9.00E-09	1.33E-04	0.18	8.80E-19
	pyterlite	2.01E-09	2.96E-05	0.085	2.20E-19
	viborgite	1.34E-08	1.98E-04	0.18	1.00E-18
	viborgite	3.20E-09	4.72E-05	0.105	1.50E-17
	viborgite	1.60E-09	2.36E-05	0.065	4.00E-19
(Li & Dong, 2009)	Berea sandstone	6.50E-10	1.29E-01	18.85	2.60E-13
	Berea sandstone	7.58E-10	1.50E-01	18.85	2.60E-13
	Berea sandstone	5.60E-10	1.11E-01	18.2	1.61E-13
	Berea sandstone	6.30E-10	1.25E-01	18.2	1.61E-13
	Berea sandstone	7.58E-10	1.50E-01	18.32	1.58E-13
	Berea sandstone	6.80E-10	1.35E-01	18.32	1.58E-13
(Li & Dong, 2010)	-	5.80E-10	2.25E-01	21.73	1.80E-12

		6.32E-10	2.46E-01	22.53	1.51E-12
		9.40E-10	3.64E-01	17.08	1.17E-13
		5.83E-10	2.28E-01	18.92	2.24E-13
		5.96E-10	2.32E-01	17.5	7.90E-14
		8.30E-10	3.23E-01	18.85	2.60E-13
		6.92E-10	2.70E-01	18.2	1.61E-13
		8.82E-10	3.37E-01	18.32	1.58E-13
(Chen et al., 1977)	-	-	2.40E-02	14.1	9.97E-15
			6.74E-02	12.7	4.84E-14
			1.59E-02	19.1	3.32E-13
(Boving & Grathwohl, 2001)	limestone	2.54E-10	1.37E-01	42.6	-
	limestone	2.88E-10	1.55E-01	42.7	
	limestone	7.22E-12	3.88E-03	7.4	
	limestone	2.57E-12	1.38E-03	6.4	
	limestone	9.96E-13	5.35E-04	3.3	
	limestone	2.24E-12	1.18E-03	3.9	
	limestone	6.78E-13	3.63E-04	3.7	

	limestone	1.24E-12	6.67E-04	3.7	
	limestone	3.32E-11	1.78E-02	19.2	
	limestone	3.13E-11	1.68E-02	19.2	
	limestone	1.15E-10	6.18E-02	22.9	
	limestone	7.32E-11	3.94E-02	24	
	limestone	9.48E-12	5.10E-03	10	
	limestone	2.64E-12	1.42E-03	10.6	
	limestone	2.34E-12	1.26E-03	10.2	
	sandstone	1.69E-11	9.09E-03	12.5	
	sandstone	1.70E-11	9.14E-03	11	
	sandstone	3.40E-11	1.83E-02	15.5	
	sandstone	6.50E-11	3.49E-02	17.5	
	sandstone	3.95E-11	2.12E-02	16	
	sandstone	4.50E-11	2.42E-02	16	
	sandstone	2.65E-11	1.42E-02	20.5	
	sandstone	2.50E-11	1.34E-02	19	
	sandstone	4.40E-11	2.37E-02	23	

	sandstone	5.15E-11	2.77E-02	23	
	sandstone	6.75E-11	3.63E-02	24	
	sandstone	7.10E-11	3.82E-02	25	
	sandstone	6.50E-11	3.49E-02	24.5	
	sandstone	6.04E-11	3.25E-02	24.5	
(Peng et al., 2012)	sedimentary	7.36E-07	3.61E-02	39.6	-
	sedimentary	9.53E-07	4.67E-02	45.6	
	sendimentary	3.69E-07	1.81E-02	38	
	sendimentary	3.00E-07	1.47E-02	9.3	
	sendimentary	5.31E-07	2.60E-02	17.4	
	construction material	1.44E-06	7.06E-02	20.3	
	repacked sediment	3.93E-06	1.93E-01	43.1	
	repacked sediment	3.53E-06	1.73E-01	42.4	
	repacked sediment	3.92E-06	1.92E-01	43.1	
	repacked sediment	3.83E-06	1.88E-01	43.1	
	repacked sediment	4.45E-06	2.18E-01	47.1	
	repacked silica sand	3.10E-06	1.52E-01	43.1	

	repacked silica sand	4.69E-06	2.30E-01	52.2	
	repacked silica sand	4.09E-06	2.00E-01	52.5	
	repacked silica sand	2.21E-06	1.08E-01	42	
	repacked silica sand	3.93E-06	1.93E-01	44	
	repacked silica sand	4.09E-06	2.00E-01	37.8	